AD-A154 703 STRAIN RATE SENSITIVITY ESTIMATION FROM HIGH VELOCITY IMPACT DATA(U) AIR FORCE INST OF TECH WRIGHT-PATTERSON AFB OH SCHOOL OF ENGINEERING M H BEDNAREK MAR 85 1/1

UNCLASSIFIED AFIT/GAE/AA/85M-2 F/G 20/11 NL

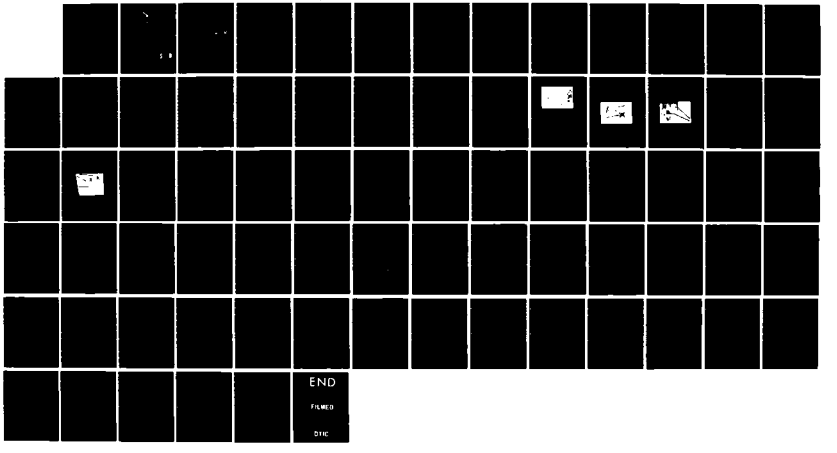

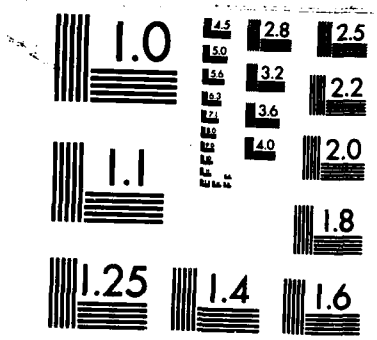

MICROCOPY RESOLUTION TEST CHART
NATIONAL BUREAU OF STANDARDS-1963-A

STRAIN RATE SENSITIVITY ESTIMATION FROM HIGH VELOCITY IMPACT DATA

THESIS

Michael H. Bednarek
Captain, USAF
AFIT/GAE/AA/85M-2

DEPARTMENT OF THE AIR FORCE
AIR UNIVERSITY
AIR FORCE INSTITUTE OF TECHNOLOGY

Wright-Patterson Air Force Base, Ohio

AFIT/GAE/AA/85M-2

STRAIN RATE SENSITIVITY ESTIMATION FROM HIGH VELOCITY IMPACT DATA

THESIS

Michael H. Bednarek
Captain, USAF
AFIT/GAE/AA/85M-2

Approved for public release, distribution unlimited

AFIT/GAE/AA/85M-2

STRAIN RATE SENSITIVITY ESTIMATION FROM HIGH VELOCITY IMPACT DATA

THESIS

Presented to the Faculty of the School of Engineering
of the Air Force Institute of Technology
Air University
in Partial Fulfillment of the
Requirements for the Degree of
Master of Science in Aeronautical Engineering

Michael H. Bednarek, B.S.
Captain, USAF

PREFACE

The purpose of this project was to expand on a previously developed method of estimating strain rate sensitivity factors through relatively simple ballistic impact experiments. This effort was designed to duplicate tests as an independent check of published results, expand on the materials tested to include more aerospace orientated materials, and explore elevated temperature and heat treatment effects on strain rate sensitivity.

I would like to acknowledge the sponsorship and support of the Test and Evaluation Group, Flight Vehicle Protection Branch, Vehicle Equipment Division of the Air Force Wright Aeronautical Laboratories.

The following personnel deserve special thanks: Major Ralph C. Kanko, for his support during his tenure as Chief, Test and Evaluation Group; Chalmer Cruze and William Studebaker for ballistic launcher expertise; Doug Coppess for his instrumentation magic; and to Lt Col George W. Watt for his assistance as thesis advisor. Final thanks to Annie Bolus, for without her typing skills you wouldn't be able to read this.

Michael H. Bednarek

TABLE OF CONTENTS

LIST OF FIGURES

LIST OF TABLES

LIST OF SYMBOLS

SYMBOL	DESCRIPTION	UNIT
d	Crater Depth-Actual	mm
d_c	Crater Depth-Calculated	mm
E_o	Impact Energy	Joules
e	Average Strain	mm/mm
$\dot{e}$	Strain Rate	sec^{-1}
$\dot{e}_T$	Strain Rate-Tabor Approximation	sec^{-1}
$\dot{e}_i$	Strain Rate-Instantaneous	sec^{-1}
F	Indenter Force	N
F_m	Mean Indenter Force	N
H	Meyer Hardness	GPa
L	Mean Deformed Distance	mm
m	Indenter Mass	kg
P_d	Dynamic Flow Pressure	GPa
R	Crater Depth Ratio (d_c/d)	
r	Indenter Radius	mm
T	Time of Impact	sec
V	Impact Velocity	m/sec
V_c	Crater Volume	m^3
V_d	Deformed Volume	m^3
V_r	Indenter Rebound Velocity	m/sec
w	Crater Diameter	mm
w_c	Calculated Crater Diameter	mm

LIST OF SYMBOLS

(con't)

x	Indenter Penetration		Distance	m
$\dot{x}$	"	"	Velocity	m/sec
$\ddot{x}$	"	"	Acceleration	m/sec^2
Y	Material Yield Stress			GPa

Abstract

This experimental study was designed to expand on the work accomplished by Sundararajan and Shewmon in estimating the strain rate sensitivity factors for various materials through the use of simple ballistic impact experiments. The study was divided into the following categories: development of an alternate method of estimating average strain rate, expand the existing data to include more relevant aerospace alloys, exlore the effect of heat treatment or elevated temperatures on strain rate sensitivity, and to duplicate tests as a verification of assumptions.

The experimental procedure involved impacting test specimens with hardened steel spheres at known velocities. The resulting crater depth and diameter can then be correlated to an average strain and time of impact, and therefore, into an estimate of average strain rate. The energy of the impacting sphere divided by the crater volume is equated to the average dynamic flow pressure.

The test results compared favorably with those obtained by Sundararajan and Shewmon. However, based on a more exact solution of time of impact, their strain rates reslted in errors approaching 30% for high strain impacts. Also, their conclusions relative to the relationship between crater relaxation profiles and elastic rebound were not confirmed for the materials tested in this study.

The materials tested generally showed a variation in dynamic hardness with increased temperature and increased hardness resulting from more severe heat treatment resulted in material less tolerant to strain rate variation. Strain rate sensitivity facators were low for the precipitation hardened alloys and intermediate for the solid solution alloys and powdered metal alloys.

STRAIN RATE SENSITIVITY ESTIMATION FROM HIGH VELOCITY IMPACT DATA

I. Introduction

High strain rate deformation is observed in such diverse actions as metal forming, foreign object damage in turbines, ballistic impacts on armour material, and cartridge case wall deformation during gun actuation. Many high strain rate experiments, such as the massive carriage/Hopkinson bar experiment described by Mok and Duffy (1), require complicated equipment and are often too time consuming to be operated routinely. Recent work by Sundararajan and Shewmon (2) has shown that data from relatively simple impact experiments can relate directly to realistic estimates of strain rate sensitivity. The method they used involved impacting target materials with hard steel spheres and measuring the resulting crater depth, diameter, and volume. From this data, an estimate of the average strain and strain rate can be obtained and used to estimate strain rate sensitivity.

This experimental study was designed to expand the work accomplished by Sundararajan and Shewmon. The study can be conveniently divided into the following categories:

a. Develop an alternate method for obtaining average strain rate. The closed form Tabor approximation for estimating the time of impact (3:132), as utilized by Sundararajan and Shewmon for estimating strain rate, is only valid at low crater depth to indenter radius ratios (The error is less than 4% when $d/r = 0.1$).

b. Expand the data base. The data published by Sundararajan and Shewmon were principally alloys little used in current aerospace structures. The metal alloys obtained for use in this project are either currently used in aerospace structures or are candidates for inclusion in future programs.

c. Test at elevated temperatures. These tests may help ascertain the effects of elevated temperatures on strain rate sensitivity of alloys normally selected for their high temperature static properties.

d. Explore the effects of heat treatment on dynamic stress-strain properties. Metals may become increasingly sensitive to strain rate variation when heat treated to increase static properties.

e. Duplicate some of the tests performed by Sundarajan and Shewmon on 304SS and 7075-T651 as an independent verification of assumptions.

(3) Upon rebound, the projectile retriggers the photoelectric screen response on channel 1.

The Nicolet oscilloscope trace is automatically digitized and the time from initial sweep trigger can be obtained directly and is accurate to within 0.001ms. The reset time for the photoelectric screen is 0.500ms thereby limiting the maximum recordable rebound velocity to 450 m/s. This was well above the maximum impact velocity of 300 m/s planned for this experiment.

Heater Assembly. The heater assembly (Fig. 8) consisted of a bank of high output, infrared lamps directed at the face of the specimen. Temperature variation was obtained by varying either the quantity or standoff distance of the heater bank. All elevated temperature tests were accomplished after the specimen heat soaked for a minimum of one hour after obtaining the desired temperature. The specimen was insulated from the target backstop in order to minimize temperature variations and target equilibrium temperature verification was obtained through the use of a Tektronic thermocouple probe.

Test Item Description

Table I lists the alloys and properties of the materials tested. All specimens were nominally 6.35mm thick, with surface finish either as received (commerically available alloys) or as machined (prototype alloys). In all cases the specimen surface lacked asperities of sufficient size to significantly effect the test results (3:61-64).

Data Collection

Impact crater diameter was obtained with a machinists' optical comparator accurate to within 0.05mm. Recorded crater diameter was the

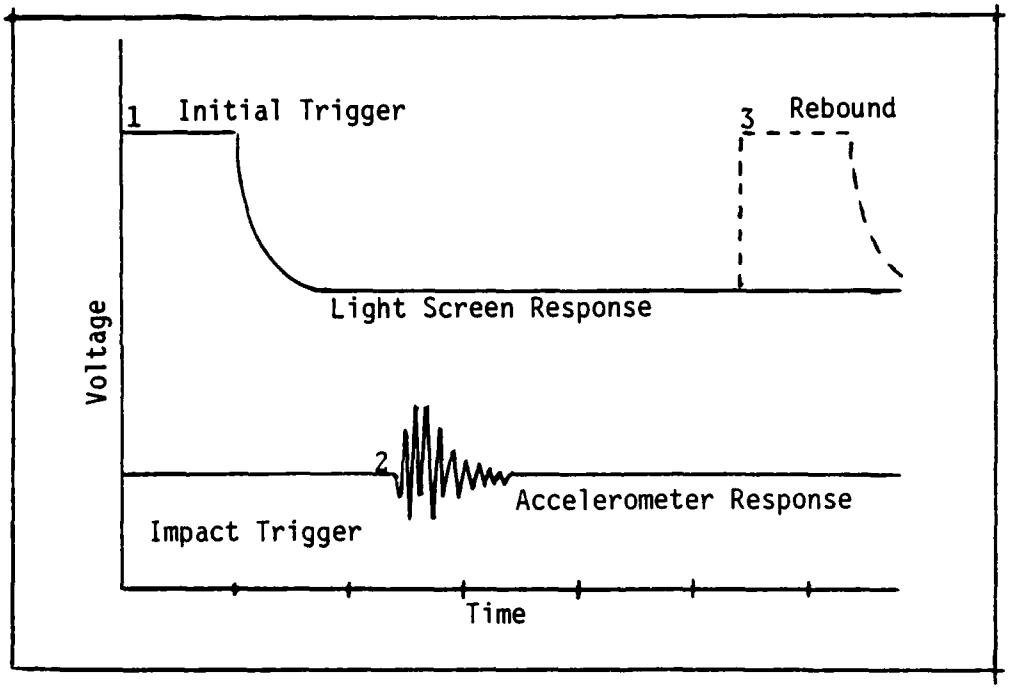

Fig. 7 Sample Nicolet Data Trace

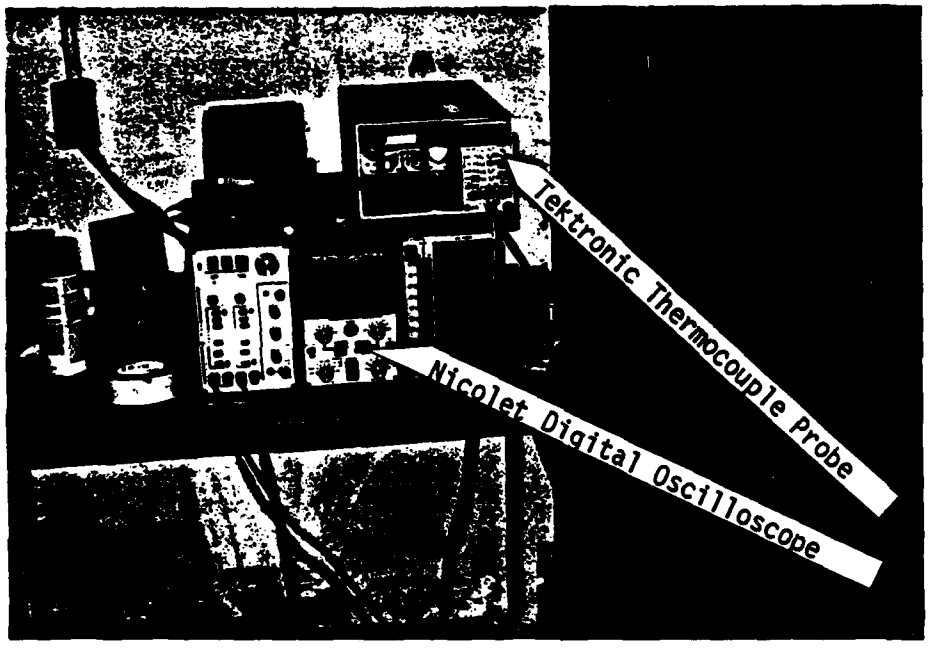

Fig. 6 Test Instrumentation

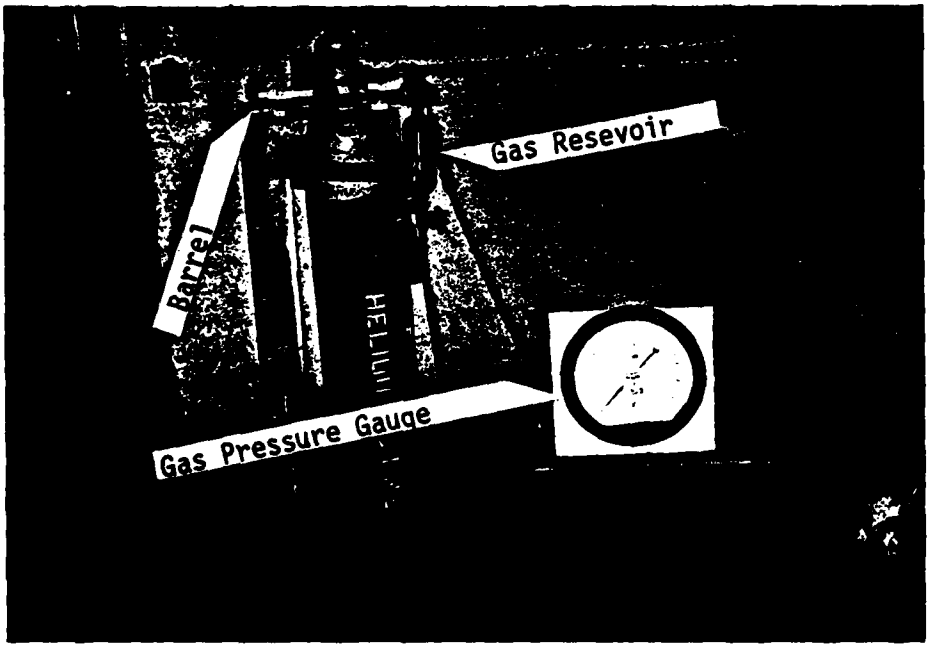

Fig. 5 High Pressure Gas Gun

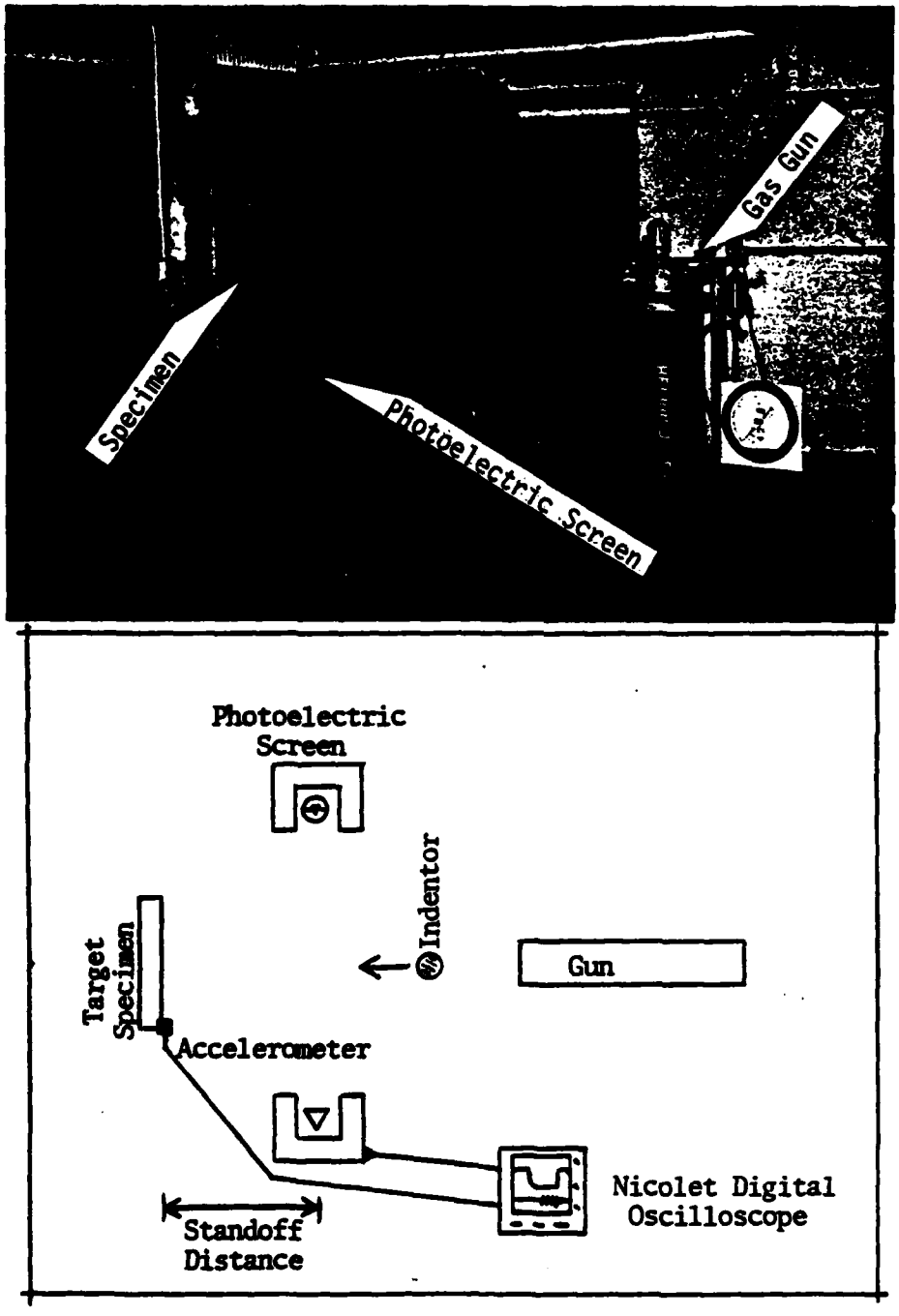

Fig. 4 Ballistic Test Apparatus and Instrumentation Diagram

III. Experimental Appratus

The ballistic test apparatus, individually described below and illustrated in Fig. 4, consisted of a smoothbore gas gun, photoelectric screen/accelerometer velocity detector, and a specimen heater assembly.

Gas Gun. The smoothbore gas gun (Fig. 5) consisted of a high pressure helium source, gas regulator/feed assembly, electrically activated firing valve, and a smoothbore barrel assembly. Barrel calibers of either 6.35mm or 12.7mm were available, with velocity repeatablity within 5 m/s. Weapon firing sequence was:

(1) Align barrel normal to impact surface

(2) Muzzle load the projectile/sabot desired

(3) Charge gas reservoir to the desired pressure

(4) Energize the gas valve solenoid to fire the weapon

Velocity Detector. The unique velocity detector fabricated for this program consisted of a photoelectric detector screen placed a short distance (variable to allow for specimen clearance) from the target plate, an accelerometer mounted on the target plate surface, and a Nicolet, two channel, high speed digitizing oscilloscope (Fig. 6). Detector operation is described below, with the subparagraph numbers matching the segments of the sample oscilloscope trace illustrated in Fig. 7.

(1) Projectile passage trips the photoelectric screen, thereby triggering the sweep of the Nicolet oscilloscope on channel 1.

(2) Projectile impact triggers the accelerometer response on channel 2.

tion of depth of penetration. Furthermore, the time to reach maximum penetration depth can be found, using $dt = dx/\dot{x}$

$$T = \int_0^d ((2/m)(E_o - P_d(\ /3)x^2(3r-x)))^{-1/2}dx \qquad (11)$$

which, if Case A applies, reduces to

$$T = 1/V \int_0^d (1-(x^2(3r-x)/d^2(3r-d)))^{-1/2}dx \qquad (12)$$

V = Impact Velocity

Equations (11) or (12) can easily be handled by computer numerical methods.

Now knowing the average strain from Equation (3) and the time of impact from Equation (11) or (12), an average strain rate can be computed.

$$\dot{e} = e/T \qquad (13)$$

Substituting Equation (7) into (3) results in

$$e = (2rx-x^2)^{1/2}/10r \qquad (14)$$

The differentiating Equation (14) with respect to time gives

$$\dot{e}_i = (r-x)\dot{x}/(10r(2r-x)^{1/2}x^{1/2}) \qquad (15)$$

As can be seen from Equation (15), the instantaneous strain rate during the impact process starts at infinity due to geometric effects and decays to zero as the velocity decreases at the end of the impact process. In reality, the initial strain rate, although high, would not be infinite because of material constraints.

Given the equations presented in the preceding paragraphs for obtaining average values for strain (e), strain rate ($\dot{e}$), static hardness (H) and dynamic flow pressure (P_d), one may now derive strain rate sensitivity factors from data collected from relatively simple ballistic experiments.

depth and at time t after the impact gives

$$t = \pi r(m/2\pi r P_d)^{1/2}/2 \qquad (6d)$$

The major error in this time of impact equation is the first order approximation of the crater diameter as $(2rx)^{1/2}$, where in fact the true crater diameter is given by

$$w_c = (2rx - x^2)^{1/2} \qquad (7)$$

therefore, the mean decelerating force becomes:

$$F_m = \pi(2rx-x^2)P_d \qquad (7a)$$

and the more accurate motion equation is

$$M\ddot{x} + P_d\pi(2rx - x^2) = 0 \qquad (8)$$

The Tabor approximation underestimates the decelerating force by a factor of nearly two during the later stages of impact. Equation (8) is not difficult to solve to obtain $\dot{x}$; however, the energy method shown below also gives the time of impact directly.

An alternate method of obtaining a mean time of impact for fully plastic indentations is to treat the impact process as an energy balance. Assuming all energy dissipated during impact is stored as plastic strain energy in the target, the energy balance equation becomes:

Total Impact Energy	=	Kinetic Energy of Indenter During Indentation	+	Energy Dissipated During Impact
E_o	=	$1/2\ m\dot{x}^2$	+	$P_d\ (\pi x^2(3r-x)/3)$ (9)

Solving for x

$$\dot{x} = ((2/m)(E_o - P_d(\pi/3)x^2(3r-x)))^{1/2} \qquad (10)$$

Equation 10 can be used directly to give a velocity profile as a func-

of penetration. R is given by:

$$R = d_c/d \tag{5}$$

with $$d_c = r-(r^2 - w^2/4)^{1/2}$$

where r is the indenter radius. If R is greater than one, Case A prevails, while if equal to one Case B prevails. Therefore, in Case A impact conditions, one uses Equation (4) and the unrelaxed crater volume to give:

$$P_d = 3mV^2/(2\pi r d_c^2(3r-d_c)) \qquad \text{CASE A} \tag{5a}$$

where $V_c = \pi d_c^2 (3r-d_c)/3$ and $E_o = mV^2/2$

or for Case B

$$P_d = 3m(V^2-V_r^2)/(2\pi d^2(3r-d)) \qquad \text{CASE B} \tag{5b}$$

where $V_c = \pi d^2(3r-d)/3$ and $E_o = m(V^2-V_r^2)/2$

where m is the indenter mass, V is the impact velocity and V_r is the rebound velocity.

Now, given the average P_d values from Equations (5a) or (5b), two methods are available to estimate the duration of impact. Method one, developed by Tabor (3:132) and used by Sundararajan and Shewmon, equates the mean decelerating force on the impacting sphere as $2\pi rxP_d$, where x is the depth of penetration. The equation of motion for the impacting sphere becomes:

$$2\pi rxP_d = -m\ddot{x} \tag{6a}$$

$$0 = m\ddot{x} + 2\pi rxP_d \tag{6b}$$

with the solution

$$x = A \sin ((2\pi rP_d/m)^{1/2}t) \tag{6c}$$

Setting $\dot{x}=0$, i.e. the sphere comes to rest at the maximum penetration

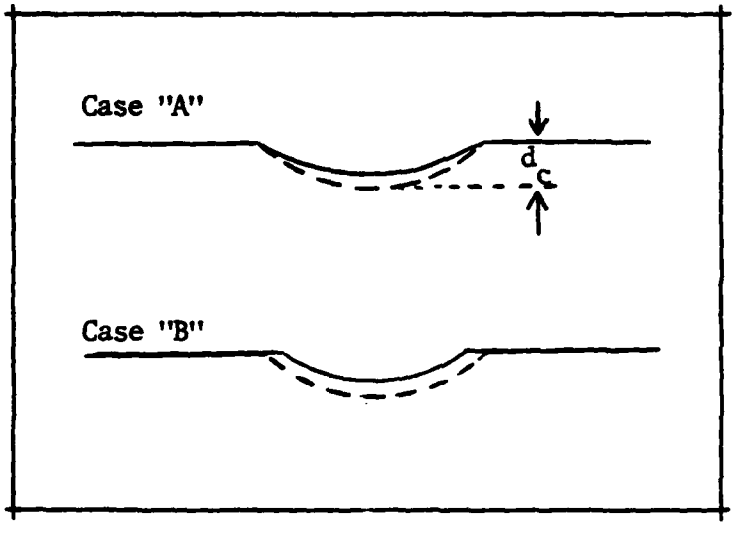

Fig. 3 Crater Relaxation Profiles

exhibit hardness variations when the rate of deformation differs from static conditions. Cristescu (4:101-119) states that, in reality, the strength of materials depends not only on the stress level and deforma- and deformation (strain), but also on time (strain rate). Fig. 2 demonstrates graphically the performance of a typical elastic-plastic material (4:112). Notice how the yield stress increases as strain rate increases.

The measure of mean dynamic hardness can be given as the ratio of the indent energy to the volume of the indentation just prior to elastic recovery. For ease in estimation, the dynamic flow pressure can be assumed constant throughout the impact process; in reality, this is not true for the following reasons:

1. Strain hardening effects exist as the target material is deformed during impact.

2. Strain rate is, as will be shown later, not constant from initial contact to final displacement.

3. Thermal softening may occur through all states of impact.

Dynamic flow pressure (P_d), is given by:

$$P_d = \frac{\text{energy of impact}}{\text{volume of indentation}} = E_o/V_c \qquad (4)$$

In the case of a spherical indenter impacting a flat surface, two methods of crater relaxation after load removal are possible (Case A and Case B of Fig. 3) (2:103). In Case A, the crater depth alone relaxes while in Case B both the crater depth and diameter relax while maintaining geometric similarity. To determine which condition exists one must obtain R, the ratio of the calculated depth to the observed depth

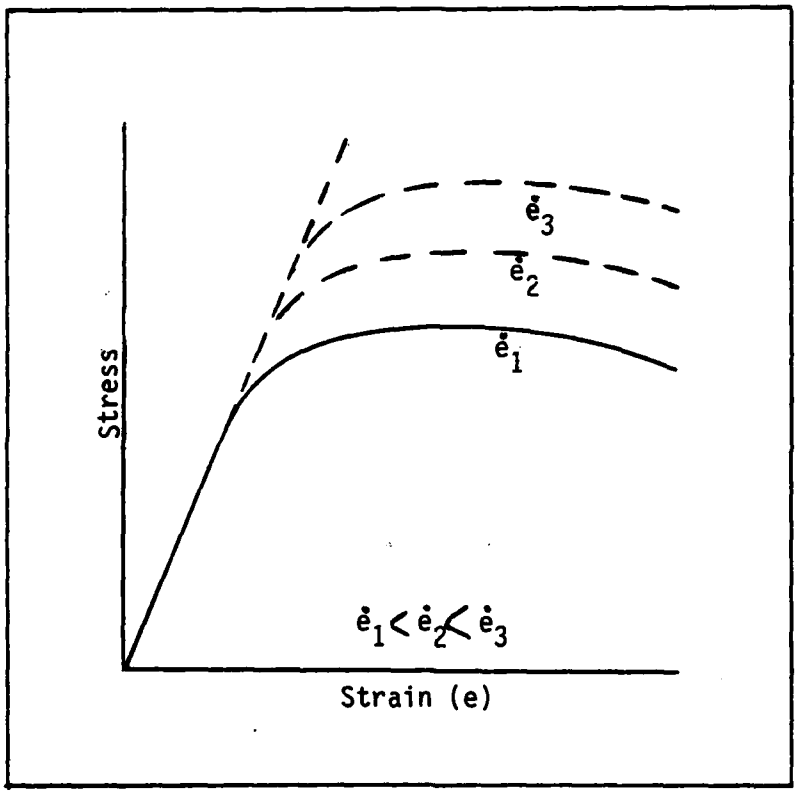

Fig. 2 Real Stress-Strain Relationships

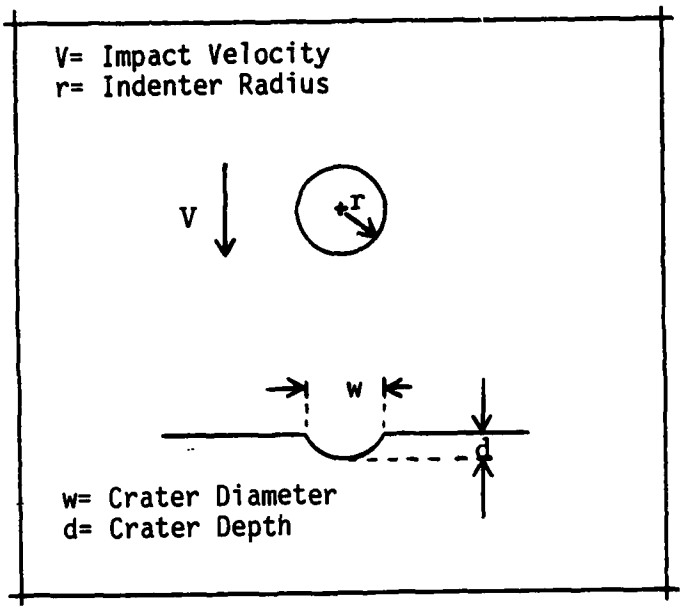

Fig. 1. Indentation Crater Parameters

II. Theory

Hardness, the ability of a material to resist plastic deformation, is one of the most commonly referenced physical properties in the selection of metal alloys for strength and abrasion resistance. One of the more common hardness tests is the indentation of the test specimen by a hard spherical indenter (Fig 1). The resulting crater depth and diameter are then related to an average hardness number. Meyer hardness (H), one of the more scientifically accurate measures of static hardness, is the ratio of the indent force to indent projected area and is given by:

$$H = 4F/\pi w^2 \tag{1}$$

where F is the indent force and w is the resulting crater diameter after load removal. Tabor, in his monograph "The Hardness of Metals" (3), developed an empirical equation from static indentation test data relating Meyer Hardness to the compressive yield stress (Y) obtained during normal stress-strain testing at an equivalent strain (e) (3:51, 73). The Tabor equations are:

$$H = CY \tag{2}$$

and

$$e = 0.1w/r \tag{3}$$

where C is a constant approximately equal to 3 and r is the indenter radius. Therefore, the Meyer hardness can be used to obtain the material compressive yield pressure, Y, at an average strain of e.

Although the Meyer Hardness is satisfactory for selection of materials for use in static applications ($\dot{e} < 10^{-2}$/sec), many materials

average value of three readings taken approximately 60° apart. Crater depth was obtained with a micrometer depth gauge accurate to within 0.0125mm, using the original, undisturbed specimen surface as the reference value. The diameter of the depth gauge tips was sufficiently small to assure accurate depth values.

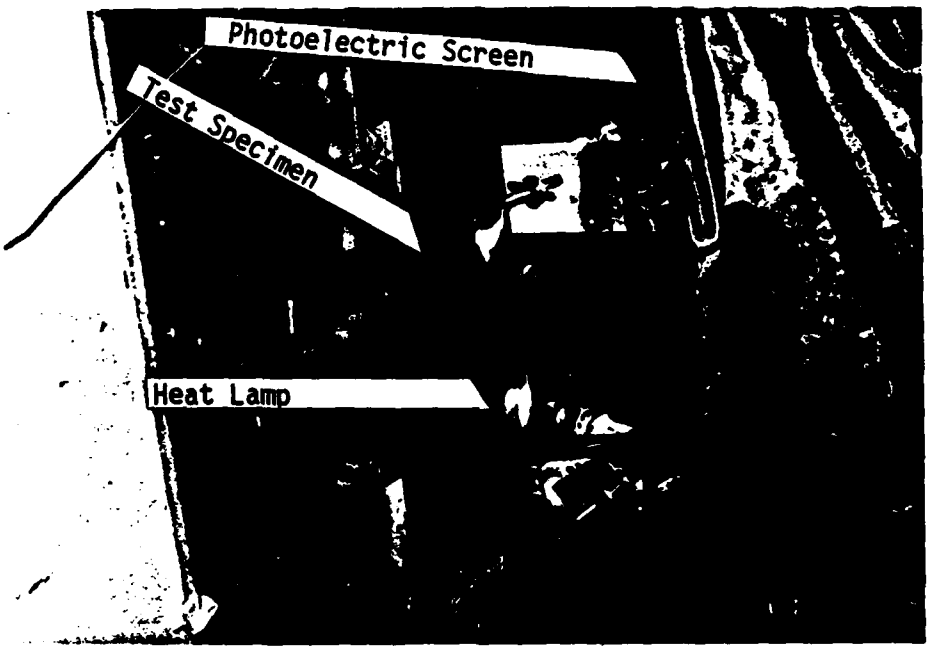

Fig. 8 Infra-Red Heater Assembly

Table I

Test Alloy Material Properties

Alloy	Yield Stress Gpa	Ultimate Stress Gpa	e, %	Note
7075-T651	.476	.531	9	b,Al-Zn-Mg-Cu Wrought Alloy
2024-T351	.324	.448	12	b, Al-Cu Wrought Alloy
Ti-6Al-4V	.999	1.10	8	b
304SS	.414	.724		
7079-T651	.421	.490	8	b, Al-Zn Wrought Alloy
2124-T3 (15% SiO)	.627	.627	.13	c, SiO whisker reinforced metal matrix
2124-T3 (25% SiO)	.535	.535	.15	c, " " "
A-703-1Y	.471	.580	.4	a, High Temp Fe (8.05%)-Ce (3.35%) PM Al
513-670-4B	.499	.554	1.	a, High Strength Fe (5.7%)-Ni (6.07%) PM Al
513-669-4B	.366	.428	1.	a, Fe (8.0%)-Ni(1.71%) PM Al
513-669-6B	.400	.444	.4	a, " " "

NOTES: a. AFWAL-TR-81-4076

b. MIL-HDBK-5D

c. Compact Tensile Tests

For all Al alloys: -T651, -T351, -T3, -1Y, -4B, -6B are heat treatment designators

IV. Test Procedures

Preliminary Impact Testing

Preliminary impact tests were performed in order to finalize the projectile diameter and to check out the test instrumentation. Projectiles were precision ground, hardened ball bearings of sufficient hardness (Rockwell "C" = 70+) to preclude plastic deformation of the indenter. Impact panels for these tests were 6.35mm 7079-T651 aluminum alloy and projectile diameters were varied from 6.35mm to 12.7mm. The specimen was inspected after impact in order to ascertain the zone of plastic deformation. The projectile diameter finally chosen was 6.35mm (m = 1.03 grams) and, except for large strain, high velocity impacts, little backface specimen deformation was apparent. A modified form of the equation listed in Appendix 1 of Sundararajan on Shewmon for estimating the thickness, L, of the deformed region is:

$$L = (5)^{1/3}r \qquad (16)$$

This equation is derived in Appendix A.

Substituting r = 3.175mm give a value of L of 5.43mm, which is less than the thickness of the target specimens.

Preliminary testing showed no indication of projectile rebound. Possible causes are:

a. Projectile lacked sufficient rebound velocity to trigger photoelectric screen.

b. Photoelectric screen failed to retrigger due to fault.

c. Angle of projectile rebound did not intersect photoelectric screen.

Electrical and mechanical checks removed (b) from the possible failure modes while paper witness panels placed forward of the light screens and less than four inches from the impact face indicated that the projectile failed to intersect the photoelectric screen upon rebound.

Therefore, a combination of (a) and (c) was the cause of this apparent error. Since the projectile boresite was centered on the 91.5cm by 61cm photoelectric detector screen and normal to the target face, gravity drop alone would cause a detector miss only if the rebound velocity was less than .75m/s. Although the value of R recorded indicated a substantial rebound velocity, the majority of the projectiles came to rest immediately below the target face. Only low rebound velocities would cause this condition. Therefore, condition (a) is justified.

Static Tests

The Meyer hardness of the specimen alloys were obtained through static indentation tests utilizing a movable crosshead Instron test machine for load application. The indenter for these test was identical to the spheres used in the dynamic tests. The test specimen was placed on the fixed crosshead and the movable crosshead was lowered to press the indenter into the target surface. Multiple tests were accomplished at different load levels in order to obtain strain hardening characteristics at low strain rates ($\dot{e}<10^{-2}sec^{-1}$). Load level readings were obtained through the internal Instron strain gauge bridge while depth and diameter of the indentation was obtained as described earlier. Static indentation results are listed in Appendix B, Table III.

Dynamic Tests

Room temperature impacts were accomplished with the photoelectric screen to target surface distance set at 0.22m, with all impacts occuring at room temperature of 25°C. Photoelectric screen to target surface distance was increased to 0.42m during elevated temperature tests in order to make room for the heater bank. Post impact inspections of the projectile diameter indicated no changes do to plastic deformation or particle erosion. Dynamic tests results are listed in Appendix B, Tables IV through XIII.

V. Results

The results of this effort compared favorably with those obtained by Sundararajan and Shewmon; however, exceptions were taken to their strain rate approximation and relationship of R with impact velocity. As shown by dynamic impact data plotted in Fig. 9, the Tabor approximation underestimated the time of impact for indentations of larger strain. Although the strain rate error appears proportional to the average strain at low strain levels ($\dot{e}$ error $\approx e$), the error exceeds 30% at indentation diameters approaching the indenter diameter. Fig. 9 also illustrates that the indentation corresponding to the maximum strain rate does not coincide with the indentation at maximum impact velocity. For the alloys tested, maximum average strain rate occurred when the dynamic indentation gave 15-17% average strain ($w/d \approx 1.6$). Of the two crater relaxation profiles used by Sundararajan and Shewmon, Case A appeared most applicable to all the dynamic testing. However, their assumption that R should be greater than one and approach one at higher impact velocities was not justified by the data. As Fig. 12 illustrates, the relationship of R with impact velocity could either be constant with impact velocity (304SS), decrease with impact velocity (Ti-6Al-4V), or increase with impact velocity (PM 7075-T6). For 304SS the value of R remained approximately one for all impact velocities. This is similar to the Case B impact criterion, but no evidence of rebound velocity after impact was observed. In fact, a number of 304SS dynamic impacts required a light hammer tap to remove the indentor from the specimen surface.

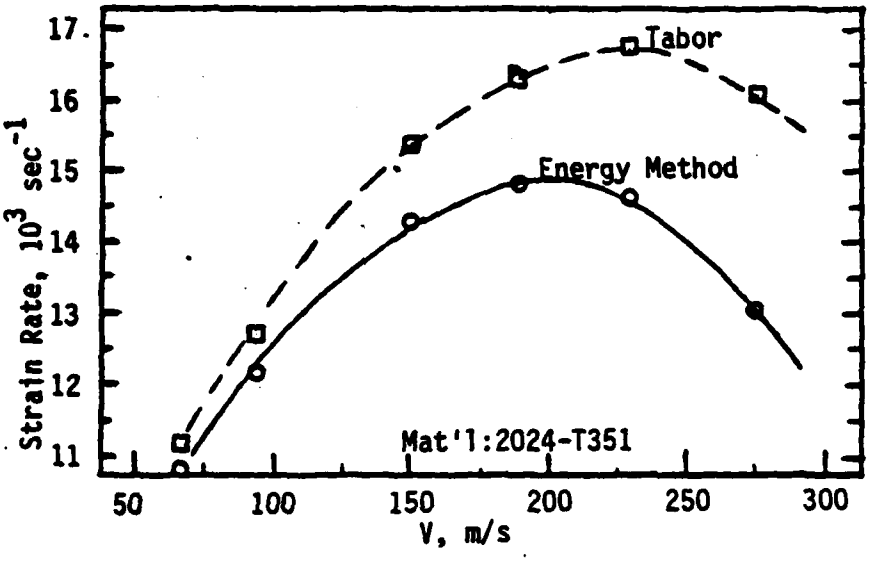

Fig. 9 Strain Rate Approximation Comparison

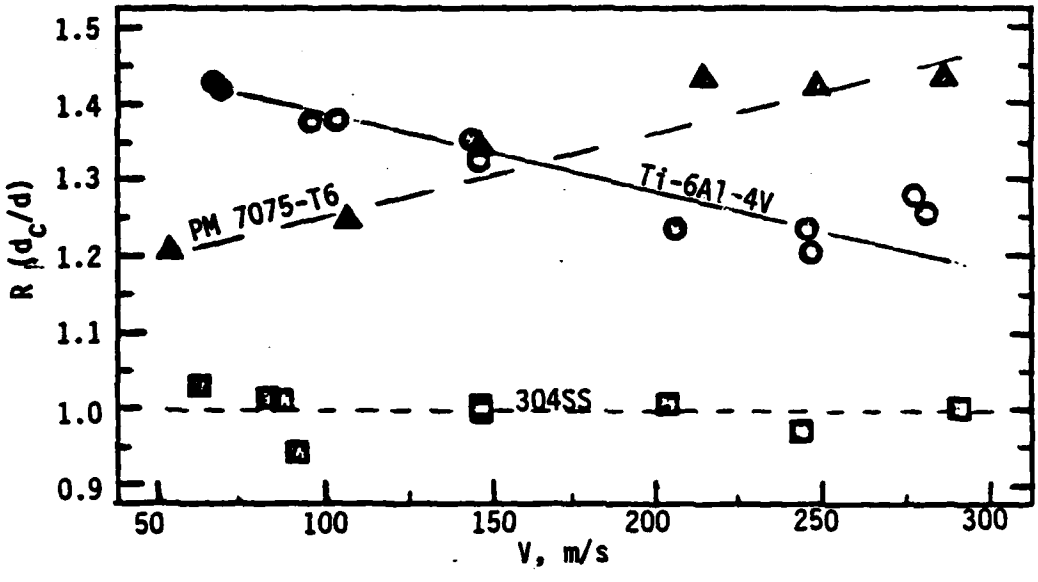

Fig. 10 Calculated to Actual Depth Ratio for Selected Alloys

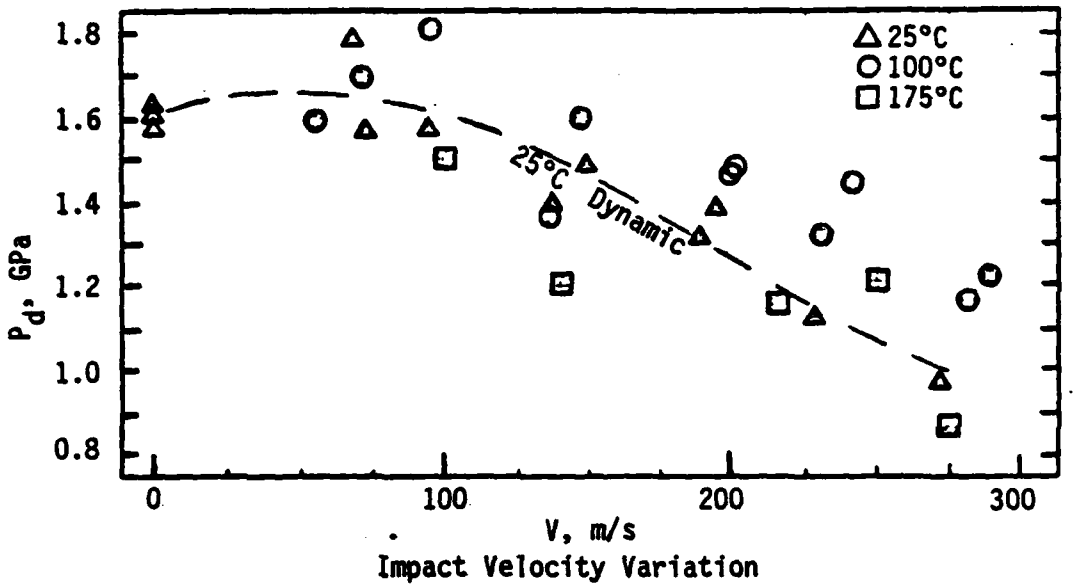

Impact Velocity Variation

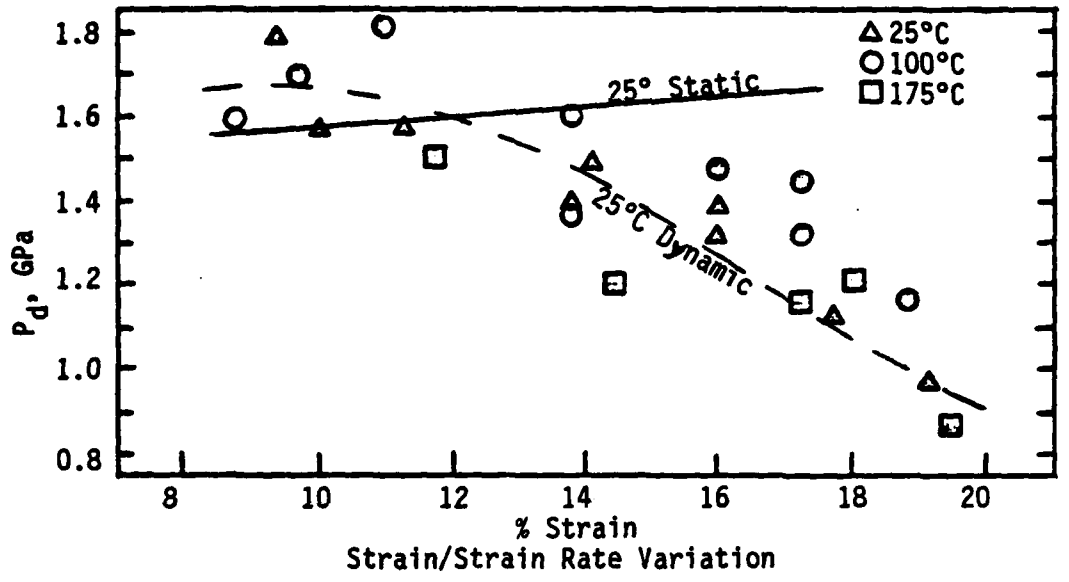

Strain/Strain Rate Variation

Fig. 11 2024-T351 Dynamic Performance

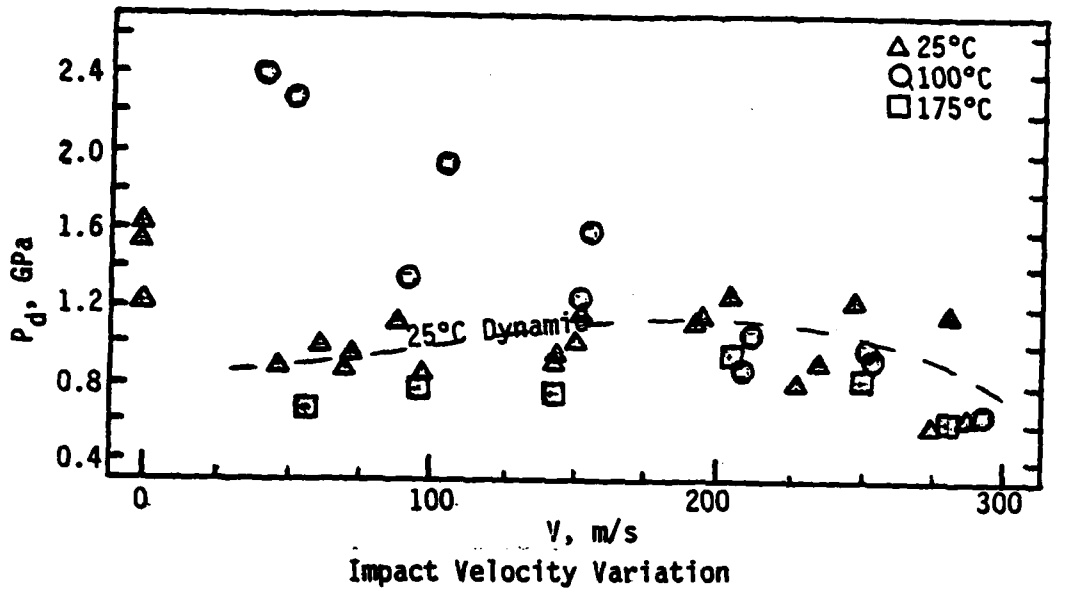

Impact Velocity Variation

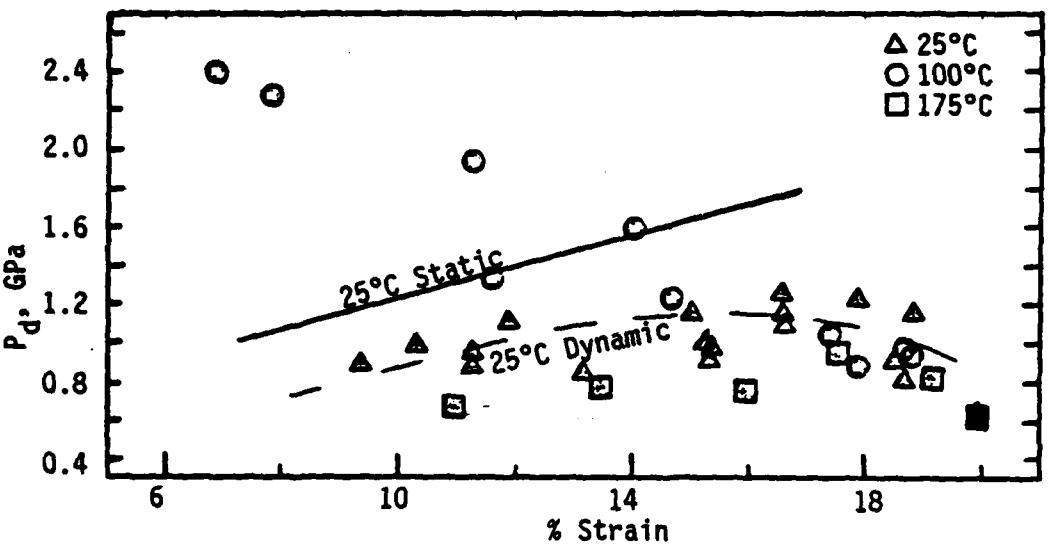

Strain/Strain Rate Variation

Fig. 12 7075-T651 Dynamic Performance

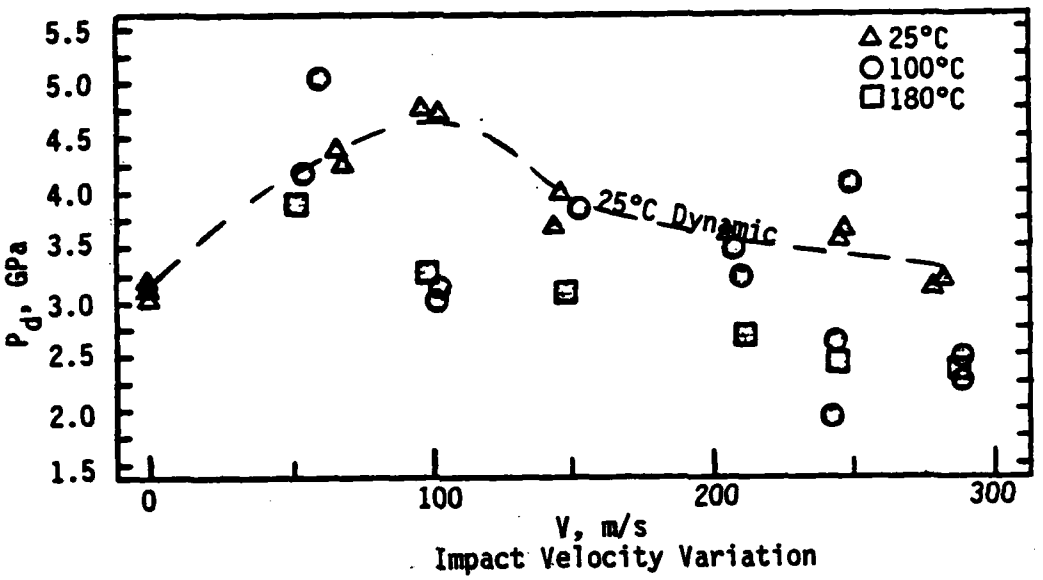

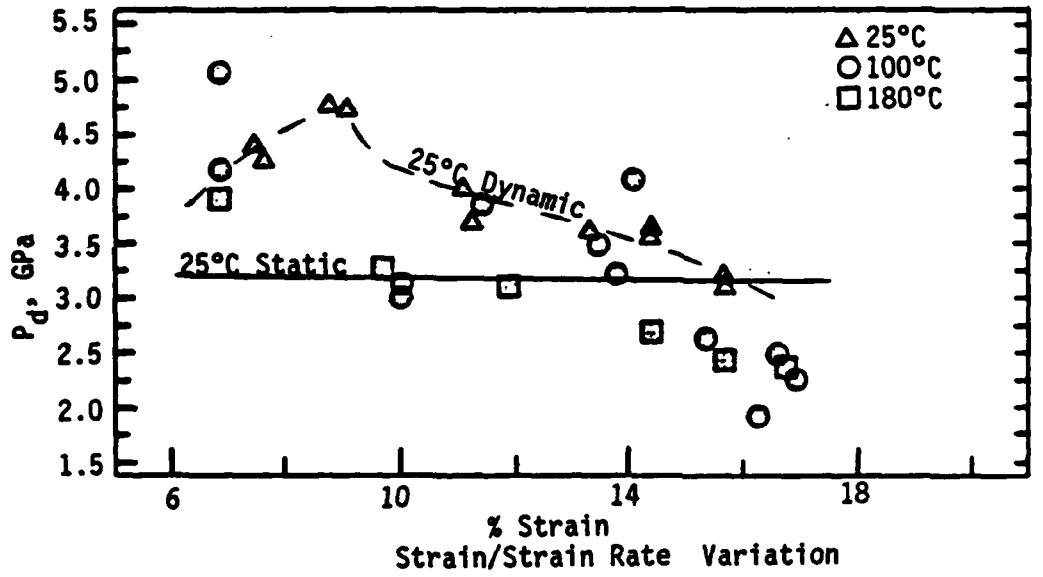

Fig. 13 Ti-6Al-4V Dynamic Performance

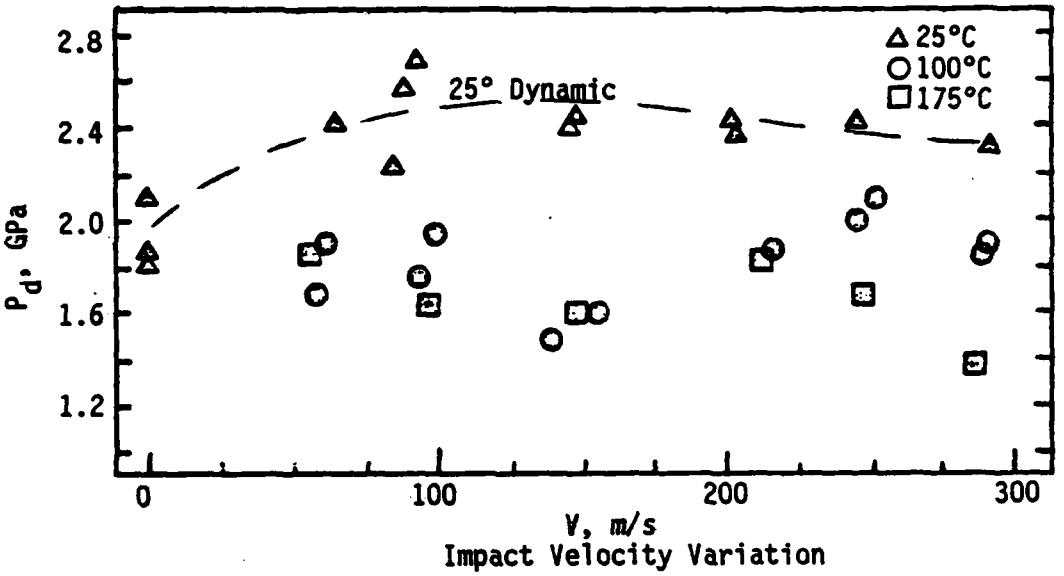

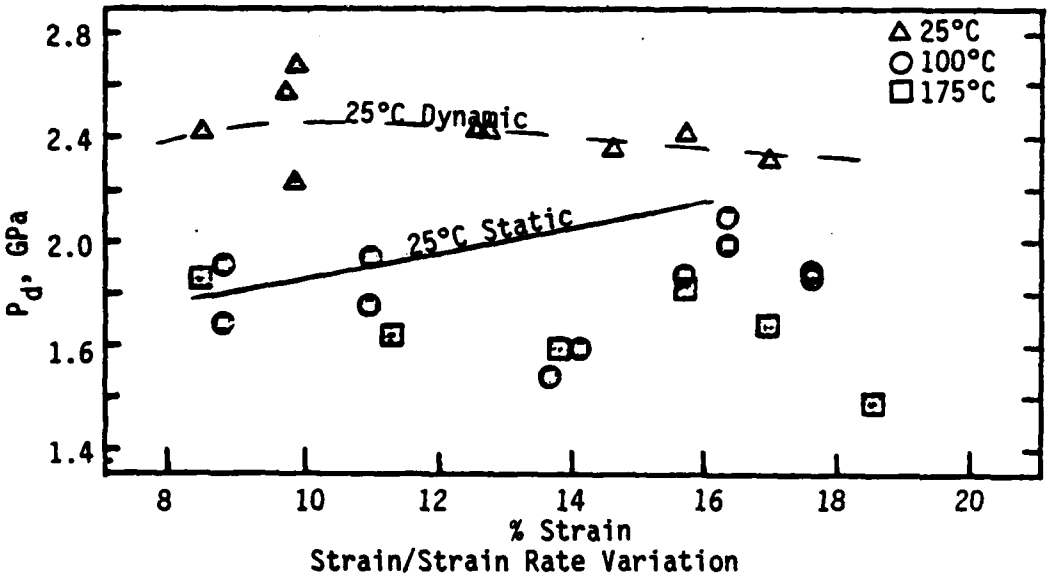

Fig. 14 304SS Dynamic Performance

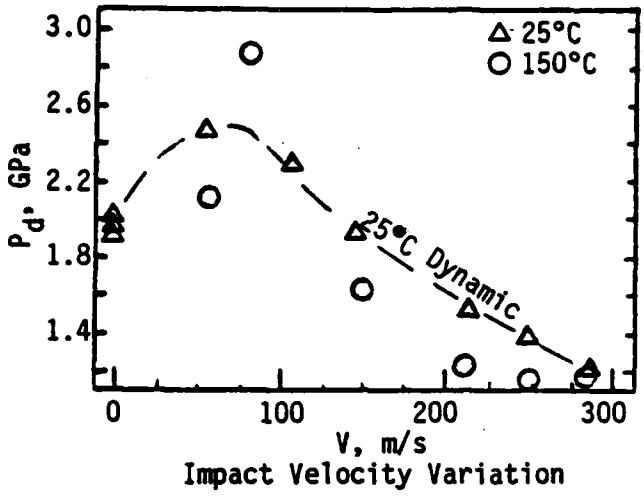

Impact Velocity Variation

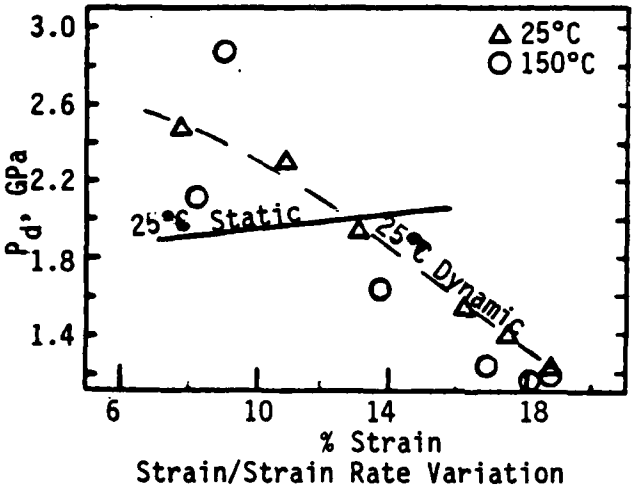

Strain/Strain Rate Variation

Fig 15. PM 7075-T6 Dynamic Performance

TABLE III (con't)

Alloy	Load, N	w,mm	e, %	H, Gpa
PM7075-T6	11,355	2.75	9	1.91
PM7075-T6	22,264	3.8	12	1.96
	33,396	4.6	14	2.01
PM A703-1Y	11,132	2.9	9	1.68
	22,264	4.1	13	1.68
	33,396	5.0	16	1.70
PM 513-670-4B	5,566	2.2	7	1.46
	11,132	2.8	9	1.81
	22,264	4.0	13	1.77
	33,396	5.0	16	1.70
PM513-669-6B	11,132	2.8	9	1.81
	22,264	4.0	13	1.77
	33,396	4.9	15	1.77
PM513-669-4B	11,132	3.0	9	1.56
	22,264	4.3	14	1.53
	33,396	5.3	17	1.51

Appendix B: Test Data

TABLE III

Static Hardness Test Data, 25°C

Alloy	Load, N	w,mm	e, %	H, Gpa
7075-T651	11,132	3.4	11	1.22
	22,264	4.3	14	1.53
	33,396	5.1	16	1.63
2024-T351	11,132	3.0	9	1.57
	22,264	4.2	13	1.60
	33,396	5.1	16	1.63
304SS	11,132	2.8	9	1.81
	23,600	4.0	13	1.87
	33,396	4.5	14	2.10
Ti-6Al-4V	11,132	2.1	7	3.21
	22,264	3.0	9	3.14
	33,396	3.7	12	3.1
2124-T3(15%SiO)	11,577	2.85	9	1.81
	22,264	3.8	12	1.96
	33,396	4.7	15	1.92
2124-T3(25%SiO)	11,132	2.7	9	1.94
	22,264	3.5	11	2.31
	33,396	4.4	14	2.19
PM7075-TO	11,355	3.8	12	1.00
	22,264	5.1	16	1.09
	33,396	5.9	19	1.22

Appendix A: Miscellaneous Equations

Deformed Region Thickness

As shown in Sundararajan and Shewmon (2.108), assuming that the deformation during indentation is similar to that occurring during a static hardness test, the volume undergoing deformation (V_d) is given by V_c/e. Using Equation (3) and given the worst case condition where the crater diameter is twice the indenter radius

$$V_d = 5V_c$$

given $V_c = 2\pi r^3/3$ and $V_d = 2\pi L^3/3$, where L is the thickness of the deformed region, this reduces to: $L = 5^{1/3} r$

Alternative Derivation of Equation (10)

As derived by Watt (5): $\ddot{x} = (-\pi P_d/m)(2rx-x^2)dx$ and $\ddot{x} = (d\dot{x}/dx)\dot{x}$

therefore: $\dot{x}d\dot{x} = (-\pi P_d/m)(2rx-x^2)dx$

integrating $\int_V^{\dot{X}} \dot{x}d\dot{x} = (-\pi P_d/m) \int_0^X (2rx-x^2)dx$

$$\dot{x}^2/2 = (V^2/2) - (\pi P_d/m)(rx^2 - x^3/3)$$

$$\dot{x} = (V^2 - (2\pi P_d\, x^2/3m)(3r-x))^{1/2}$$

or rewriting $\dot{x} = (2/m\,((mV^2/2) - (\pi P_d\, x^2/3)(3r-x)))^{1/2}$

since $mV^2/2 = E_o$, this is identical to Equation (10).

Bibliography

1. C. H. Mok and J. Duffy, "The Dynamic Stress-Strain Relation of Metals as Determined From Impact Tests with a Hard Ball". Int. J. Mech. Sci, V.7, 1965.
2. G. Sundararajan and P. G. Shewmon, "The Use of Dynamic Impact Experiments In the Determination of the Strain Rate Sensitivity of Metals and Alloys", Acta Metal, V.31, 1983.
3. D. Tabor, The Hardness of Metals, Clarendon Press, Oxford, England, 1951.
4. N. Cristescu, Dynamic Plasticity, North Holland Publishing Co., Amsterdam, 1967.
5. G. W. Watt, Private Communication, Air Force Institute of Technology, Wright-Patterson AFB, OH, 1 May 84 thru 1 Feb 85.
6. Air Force Wright Aeronautical Laboratories, Powder Metal Alloy Data, AFWAL-TR-81-4076, Wright-Patterson AFB OH, 1981.

VI. Conclusion and Recommendations

The technique developed by Sundararajan and Shewmon, with the few exceptions noted, proved to be an easily applied method of estimating strain rate sensitivity. Although limited by strain-strain rate interaction and thermal softening at higher impact velocities, the test procedure produced data consistent with known properties. A refinement to this test method would be to impact the specimen with spheres of varying diameters, keeping the relative penetration depth constant (w/d = constant). Fixing the relative depth would keep the average strain constant, thereby, only the effective strain rate would change. Furthermore, keeping the impact velocity low would substantially reduce the effect of thermal softening. The revised test method, however, would naturally limit the maximum strain and minimum thickness of the specimen in question.

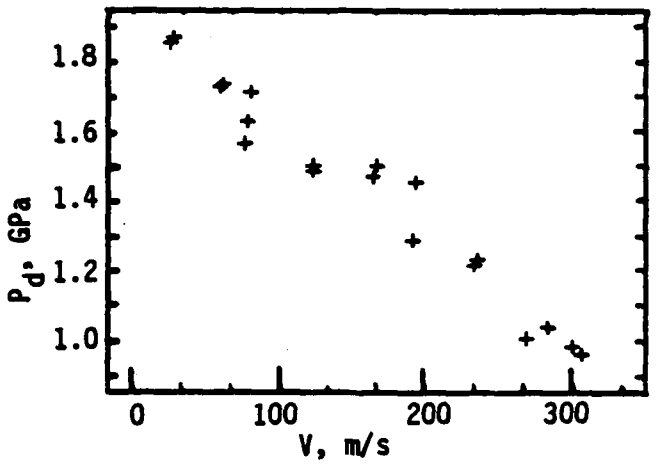

Impact Velocity Variation

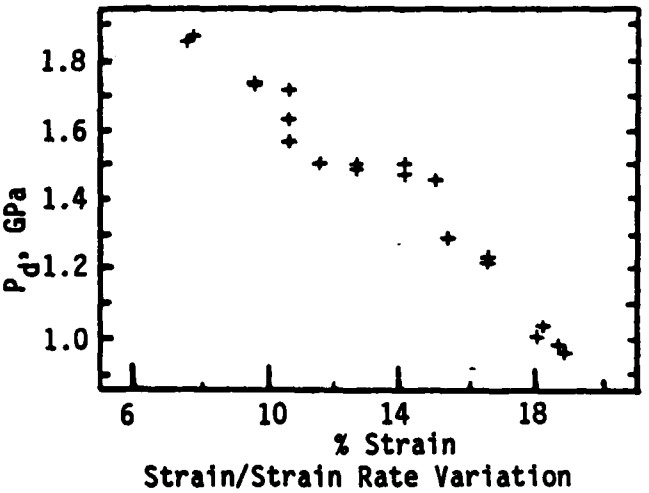

Strain/Strain Rate Variation

Fig. 22 7079-T651 Dynamic Performance

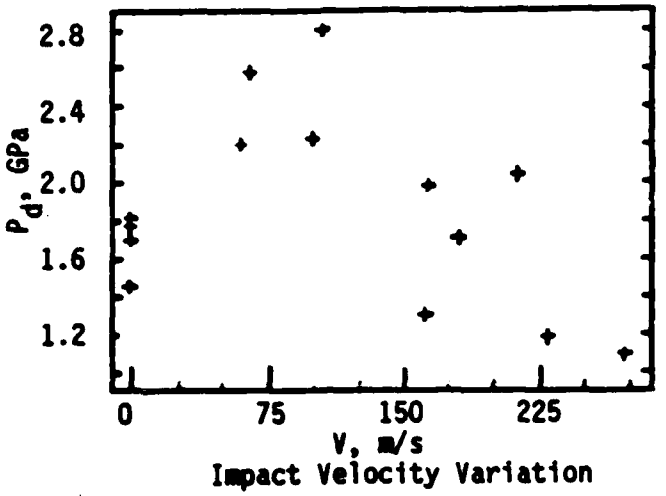

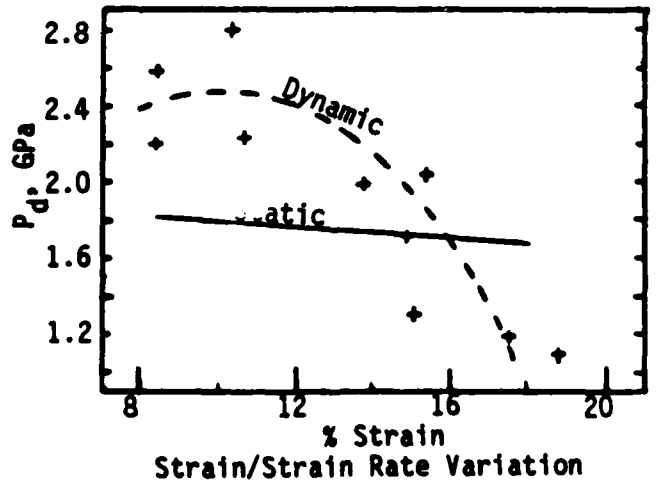

Fig. 21 PM 513-560-4B Dynamic Performance

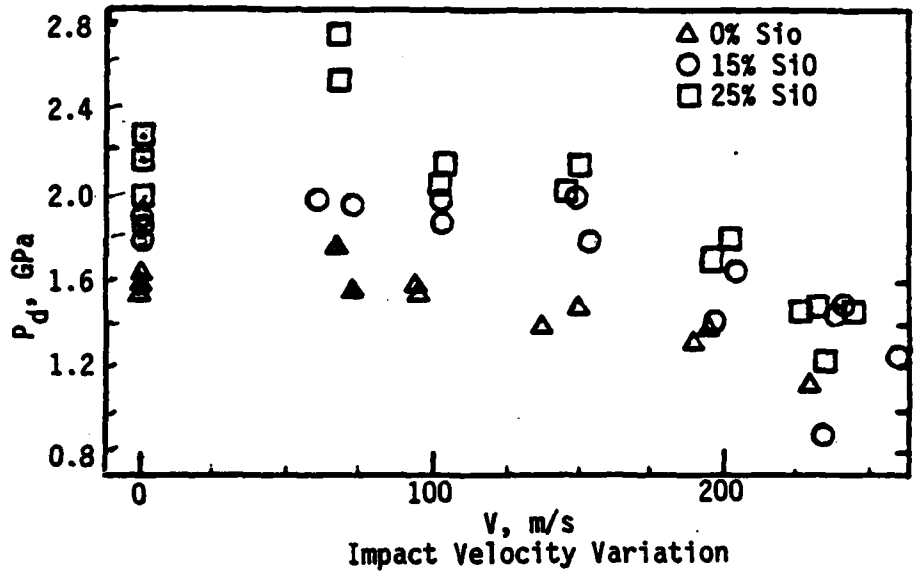

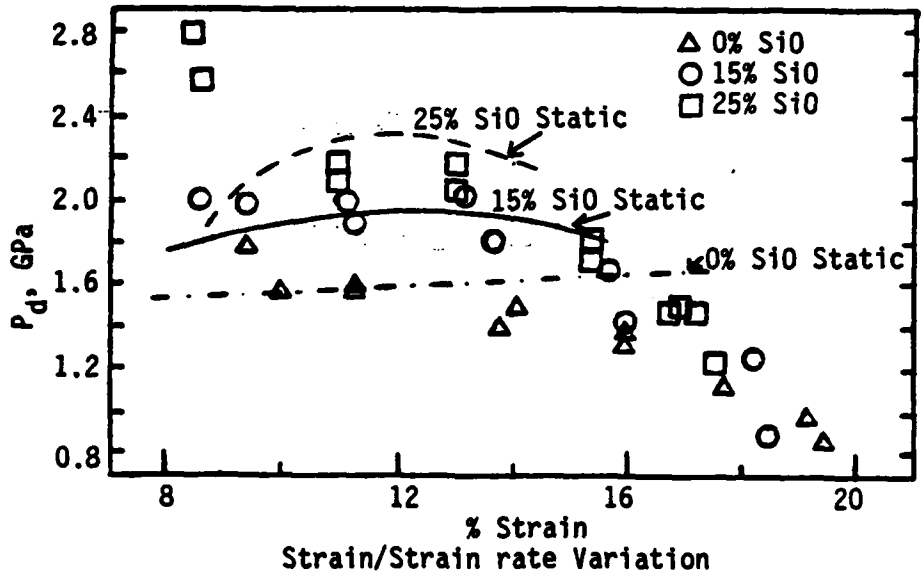

Fig. 20 2124-T3 SiO Metal Matrix Dynamic Performance

values occur. Conversely, in the softer state the alloy would have a flat strain response, with dynamic properties remaining essentially constant until softening at high strains.

All alloys, with the noted exception of the 7075-T651 alloy tested, exhibited a degree of strain rate sensitivity. Table II gives the relative ratios of dynamic to static flow pressure, P_d/H, at the strain rate giving maximum P_d and with the static values taken at the same mean strain. As noted by Sundararajan and Shewmon, the precipitation hardened wrought alloys exhibited weak strain rate sensitivity (P_d/H 1-1.2) while the solid solution alloys exhibited intermediate strain rate sensitivity (P_d/H=1.5). The powdered metallurgy aluminum alloys, although chemically similar to the precipitation hardened alloys, exhibited intermediate strain rate sensitivity due to the method used in manufacturing.

The silicon whisker (SiO) reinforced 2124-T3 metal matrix was susceptible to dynamic flow presssure reductions at low strain levels, with the dynamic hardness approaching that of the parent alloy at high strain levels (e>16%) (Fig. 20). This reduction in dynamic hardness was apparently related to the percentage of whiskers. This was expected due to the brittle nature of the SiO reinforcement. The high strength candidate powdered alloy, Fig. 21, shattered at strains above 14% during dynamic testing while no cracking appeared during static indentations at the same strain. The P_d values given for 513-670-4B above 10% strain were obtained from data taken after specimen reassembly; this alloy was extremely sensitive to shock loadings.

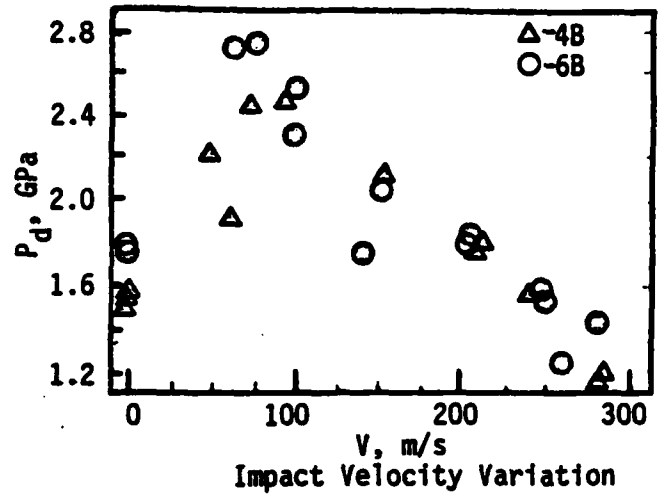

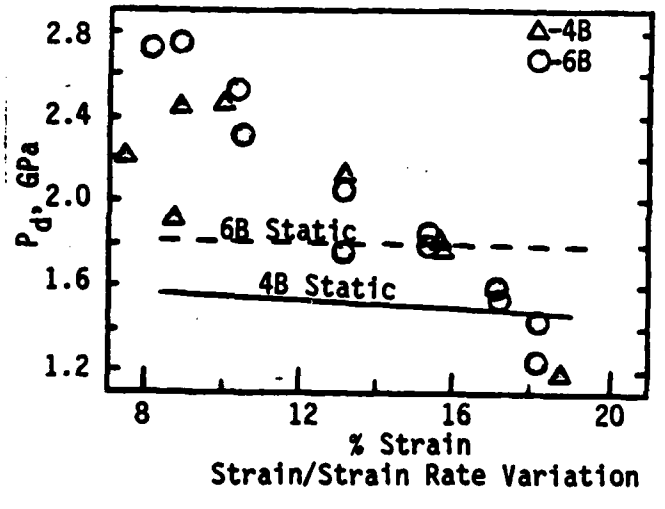

Fig 19. PM 513-670-4B/6B Dynamic Performance

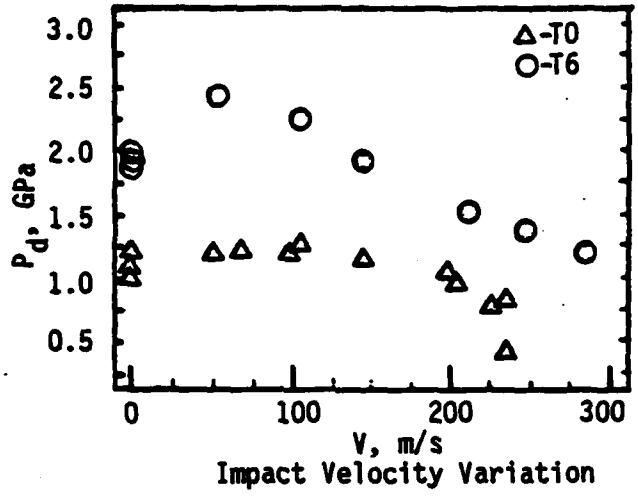

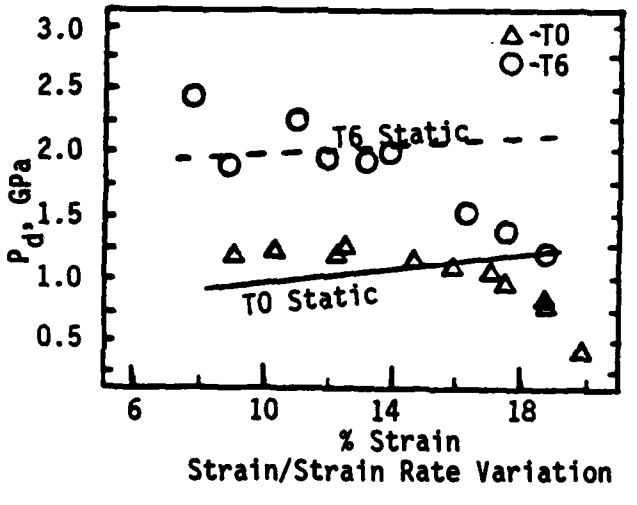

Fig 18. PM 7075-T0/T6 Dynamic Performance

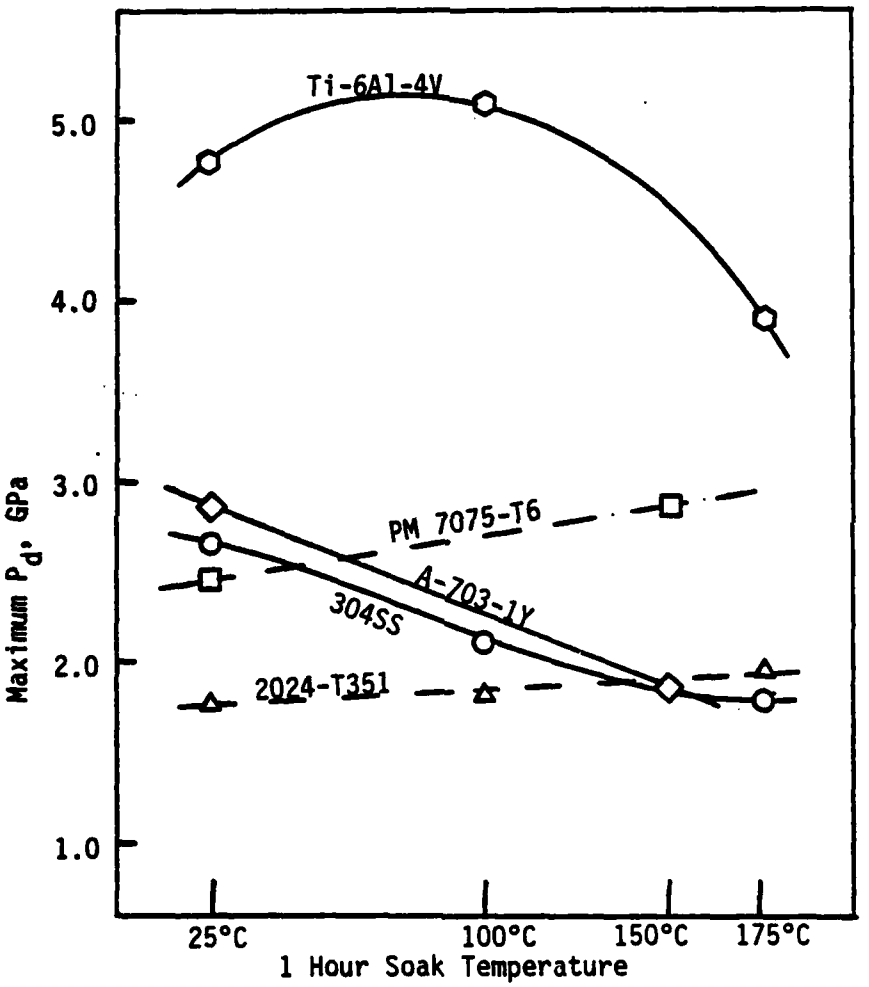

Fig 17. Maximum P_d vs Soak Temperature

All of the alloys tested at elevated temperatures, showed a variance in dynamic hardness with increased temperature (Figs. 11 thru 16). As illustrated in Fig. 17, the conventional composition 2024-T351 and PM 7075-T6 showed an increase in dynamic hardness with increased temperature while the A-703-1Y and 304SS showed a decrease with increased temperature, with the Ti-6A-4V showing an initial increase to 100°C with a decrease thereafter. The increases shown by PM 7075-T6 and 2024-T351 appears to be the result of accelerated aging at the higher soak temperatures. Of particular note was the property variation of the commercially obtained 7075-T651 plate when tested at 100°C and 175°C (Fig 14). At room temperature the static hardness was below that of the 2024-T351 alloy, however, when the plate temperature was increased to 100°C the dynamic flow pressure increased 2.4 times the ambient value. Furthermore, when heat soaked to 175°C, the alloy reverted to its room temperature properties. In order to recheck the findings on the 7075-T651 alloy, the ambient temperature tests were repeated and the specimen was submitted to quality assurance for evaluation. The ambient temperature values remained unchanged and the quality analysis showed the specimen deficit in hardness over the required values (Rockwell "B" of 90 vs 100 as called out in MIL-H-6086F). The most likely cause was incorrect heat treatment/aging during the manufacturing process. The abnormality in heat treatment adversely effected the expected variation in dynamic hardness with temperature.

Modifying the heat treatment to improve the static material strength will also increase the dynamic flow pressure (Figs. 18 and 19). However, these heat treatments would reduce the average strain where peak flow

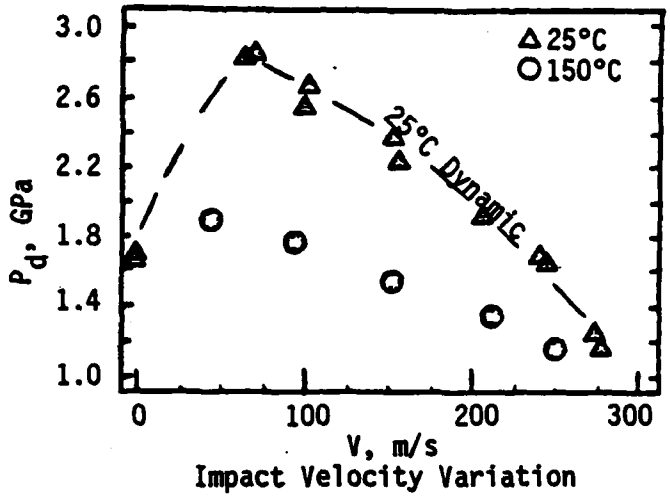

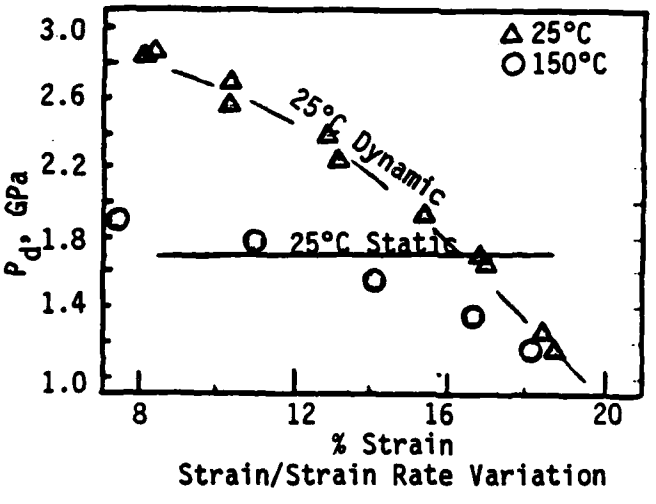

Fig. 16 PM A-703-1Y Dynamic Performance

TABLE IV

7079-T651

Dynamic Test Data, 25°C

V,m/s	w,mm	d,mm	R	e%	P_d,GPa	$\dot{e}_t$, $10^3 sec^{-1}$	$\dot{e}$, $10^3 sec^{-1}$
149.8	4.5	.72	1.3	14	1.47	15.2	14.2
151.2	4.5	.74	1.3	14	1.50	15.4	14.4
172.9	4.8	.86	1.3	15	1.45	16.1	14.9
203.	5.3	1.03	1.4	17	1.23	16.4	14.7
202.1	5.3	1.00	1.4	17	1.22	16.3	14.7
239.	5.8	1.03	1.8	18	1.04	16.5	14.2
229.1	5.8	1.02	1.8	18	1.00	16.1	14.0
252.6	6.0	1.45	1.4	19	.99	16.5	14.0
256.9	6.0	1.46	1.5	19	.96	16.4	13.9
171.	4.9	.86	1.3	15	1.29	15.5	14.2
171.	4.9	.77	1.5	15	1.29	15.5	14.2
119.5	4.1	.55	1.3	13	1.50	13.9	13.1
118.8	4.1	.55	1.3	13	1.48	13.8	13.1
119.5	3.7	.44	1.4	12	2.23	15.4	14.8
85.2	3.4	.37	1.3	11	1.62	12.1	11.7
83.7	3.4	.39	1.3	11	1.57	11.9	11.5
87.5	3.4	.39	1.3	11	1.71	12.4	12.0
72.6	3.1	.30	1.3	10	1.73	11.4	11.1
48.1	2.5	.19	1.3	8	1.87	9.5	9.4
46.	2.5	.19	1.3	8	1.86	9.3	9.1

TABLE V

2024-T351

Dynamic Test Data

V,m/s	w,mm	d,mm	R	eZ	P_d,GPa	$\dot{e}_t$, $10^3 sec^{-1}$	$\dot{e}$, $10^3 sec^{-1}$	T,°C
68.6	3.0	.33	1.1	9	1.78	11.2	10.9	25
73.6	3.2	.36	1.2	10	1.57	11.2	10.8	
94.8	3.6	.49	1 1	11	1.58	12.6	12.1	
95.4	3.6	.50	1.1	11	1.60	12.7	12.2	
138.6	4.4	.82	1.1	14	1.39	14.5	13.6	
150.7	4.5	.82	1.1	14	1.49	15.3	14.3	
195.6	5.1	1.17	1.1	16	1.39	16.8	15.2	
190.6	5.1	1.17	1.1	16	1.32	16.3	14.8	
276.4	6.2	1.63	1.5	20	.86	16.1	13.1	
273.7	6.1	1.94	1.2	19	.97	16.8	13.9	
71.7	3.1	.34	1.2	10	1.70	11.3	11.0	100
56.2	2.8	.29	1.1	9	1.60	9.9	9.6	
95.8	3.5	.52	1.0	11	1.82	13.1	12.7	
148.8	4.4	.84	1.1	14	1.61	15.6	14.6	
137.4	4.4	.8	1.1	14	1.37	14.4	13.5	
202.3	5.1	1.21	1.1	16	1.48	17.3	15.6	
201.7	5.1	1.19	1.1	16	1.47	17.3	15.7	
243.1	5.5	1.56	1.0	17	1.45	18.5	16.4	
232.2	5.5	1.51	1.0	17	1.33	17.7	15.6	
283.	6.0	1.85	1.2	19	1.17	18.1	15.3	
290.5	6.0	1.95	1.1	19	1.23	18.6	15.7	

TABLE V (con't)

V,m/s	w,mm	d,mm	R	e%	P_d,GPa	$\dot{e}_t$, $10^3 sec^{-1}$	$\dot{e}$, $10^3 sec^{-1}$	T,°C
53.7	2.6	.27	1.0	8	1.98	10.2	10.0	175
101.	3.8	.53	1.2	12	1.50	12.8	12.3	
142.4	4.6	.84	1.2	14	1.20	14.1	13.1	
217.	5.5	1.39	1.1	17	1.16	16.5	14.6	
251.4	5.8	1.66	1.1	18	1.21	17.7	15.3	
276.6	6.2	1.77	1.4	20	.86	16.1	13.1	

TABLE VI

7075-T651

Dynamic Test Data

V,m/s	w,mm	d,mm	R	eZ	P_d,GPa	$\dot{e}_t$, $10^3 sec^{-1}$	$\dot{e}$, $10^3 sec^{-1}$	T,°C
288.6	6.35	1.70	1.87	20	.64	14.2	10.7	25
275.1	6.35	1.65	1.92	20	.58	13.5	10.2	
236.4	5.9	1.37	1.46	19	.91	15.7	13.4	
229.1	5.95	1.34	1.55	19	.81	15.0	12.7	
193.6	5.3	1.07	1.34	17	1.12	15.7	14.1	
196.	5.3	1.06	1.34	17	1.15	15.8	14.2	
144.3	4.9	.73	1.57	15	.92	13.1	12.0	
145.6	4.9	.78	1.48	15	.93	13.2	12.1	
97.8	4.2	.56	1.71	13	.86	10.8	10.2	
97.8	4.2	.45	1.76	13	.86	10.8	10.2	
70.6	3.6	.31	1.82	11	.87	9.4	9.0	
73.6	3.6	.33	1.68	11	.95	9.8	9.4	
42.1	2.2	.17	1.13	7	2.42	9.5	9.4	100
53.2	2.5	.24	1.08	8	2.29	10.6	10.4	
92.9	3.7	.52	1.15	12	1.34	12.0	11.5	
152.6	3.6	.57	.98	11	1.95	14.1	13.5	
156.4	4.55	.81	1.16	14	1.60	15.9	14.9	
213.	5.6	1.18	1.38	17	1.06	16.0	14.1	
210.2	5.7	1.15	1.54	18	.89	15.	13.1	
254.6	6.0	1.47	1.45	19	.95	16.3	13.7	

TABLE VI (con't)

V,m/s	w,mm	d,mm	R	e%	P_d,GPa	$\dot{e}_t$, $10^3 sec^{-1}$	$\dot{e}$, $10^3 sec^{-1}$	T,°C
252.5	5.96	1.45	1.42	18	.99	15.5	14.0	
286.7	6.35	1.71	1.85	20	.63	14.1	10.6	
293.3	6.35	1.69	1.88	20	.66	14.4	10.9	
5.8	3.5	.28	1.89	11	.66	8.0	7.7	175
97.3	4.3	.51	1.65	14	.76	10.5	9.9	
144.6	5.1	.84	1.53	16	.76	12.4	11.3	
206.7	5.6	1.26	1.34	17	.95	15.2	13.4	
252.	6.1	1.62	1.41	19	.82	15.4	12.8	
281.8	6.4	1.92	1.66	20	.61	13.9	10.5	
89.9	3.8	.39	1.62	12	1.12	11.2	10.7	25
48.5	3.	.19	2.00	9	.89	7.9	7.7	
62.3	3.3	.25	1.84	10	.99	9.1	8.8	
154.3	4.8	.70	1.56	15	1.16	14.4	13.3	
205.9	5.3	1.05	1.56	17	1.27	16.6	14.9	
248.	5.7	1.31	1.35	18	1.24	17.7	15.4	
282.3	6.0	1.56	1.36	19	1.16	18.1	15.2	
151.7	4.9	.71	1.62	15	1.01	13.8	12.6	

TABLE VII

Ti-6Al-4V

Dynamic Test Data

V,m/s	w,mm	d,mm	R	e%	P_d,GPa	$\dot{e}_t$, $10^3 sec^{-1}$	$\dot{e}$, $10^3 sec^{-1}$	T,°C
279.6	5	.95	1.3	16	3.12	24.7	22.5	25
282.8	5	.97	1.3	16	3.19	24.9	22.8	
248	5	.82	1.2	14	3.64	24.5	22.8	
246.9	4.6	.80	1.2	14	3.61	24.4	22.7	
206.5	4.3	.50	1.6	13	3.62	22.6	21.3	
206.5	4.3	.66	1.2	13	3.62	22.6	21.3	
146.8	3.6	.41	1.3	11	4/91	19.8	19.1	
145.1	3.6	.41	1.4	11	3.69	19.3	18.5	
97.1	2.8	.24	1.4	9	4.76	17.1	16.7	
103.9	2.9	.25	1.4	9	4.71	17.6	17.1	
69.7	2.5	.17	1.4	8	4.26	14.1	13.9	
67.9	2.4	.17	1.4	8	4.40	14.1	13.8	
61	2.2	.17	1.2	7	5.08	13.8	13.6	100
55.5	.2	.14	1.4	7	4.20	12.6	12.4	
102.5	3.2	.28	1.5	10	3.04	15.6	15.1	
104.4	3.2	.28	1.5	10	3.15	15.9	15.4	
153.4	3.7	.48	1.2	12	3.89	20.1	19.3	
208.2	4.3	.68	1.2	14	3.59	22.4	21.1	
211.4	4.4	.68	1.3	14	3.24	22.1	20.7	
250.2	4.5	.86	1.1	14	4.10	25.4	23.8	

TABLE VII (con't)

V,m/s	w,mm	d,mm	R	e%	P_d,GPa	$\dot{e}_t$, $10^3 sec^{-1}$	$\dot{e}$, $10^3 sec^{-1}$	T, °C
245.1	4.9	.86	1.3	15	2.64	22.2	20.4	
244	5.2	1.08	1.3	16	1.96	20.3	18.4	
289.7	5.3	1.07	1.3	17	2.51	23.4	21.0	
289.7	5.4	1.07	1.4	17	2.27	22.7	20.3	
53.4	2.2	.14	1.4	7	3.89	12.1	11.9	180
99.4	3.1	.28	1.4	10	3.26	15.6	15.2	
149	3.8	.48	1.3	12	3.08	18.6	17.8	
213	4.6	.74	1.3	14	2.69	21.1	19.6	
245.9	5.0	.90	1.4	16	2.41	21.7	19.8	
289.3	5.4	1.30	1.1	17	2.39	23.0	20.6	

TABLE VIII

304SS

Dynamic Test Data

V,m/s	w,mm	d,mm	R	e%	P_d,GPa	$\dot{e}_t$, $10^3 sec^{-1}$	$\dot{e}$, $10^3 sec^{-1}$	T, °C
292.	5.4	1.51	.99	17	2.32	22.9	20.5	25
245.9	5.	1.24	.98	16	2.41	21.7	19.8	
245.9	5.	1.26	.97	16	2.41	21.7	19.8	
204.7	4.7	1.01	1.00	15	2.36	19.9	18.5	
148.2	4	.72	.99	13	2.44	17.4	16.6	
147.8	4.	.71	1.00	13	2.42	17.4	16.5	
88.3	3.1	.40	1.01	10	2.58	13.9	13.5	
93.1	3.2	.45	.94	10	2.68	14.4	14.0	
64.2	2.7	.29	1.03	9	2.42	11.73	11.5	
85.	3.2	.41	1.01	10	2.23	13.1	12.7	
61.5	2.8	.29	1.11	9	1.91	10.8	10.6	100
57.9	2.8	.29	1.11	9	1.70	10.2	9.9	
99.2	3.5	.51	1.04	11	1.95	13.6	13.1	
94.2	3.5	.50	1.06	11	1.75	12.9	12.5	
156.3	4.5	.85	1.11	14	1.60	15.9	14.8	
139.7	4.4	.74	1.16	14	1.49	14.8	13.9	
214.1	5.	1.21	1.01	16	1.83	18.9	17.2	
217.1	5.	1.20	1.01	16	1.88	19.2	17.5	
246.6	5.2	1.4	.97	16	2.10	21.1	19.0	
291.8	5.6	1.64	1.02	18	1.90	21.5	18.9	
288.9	5.6	1.66	1.01	18	1.90	21.3	18.7	

TABLE VIII (con't)

V,m/s	w,mm	d,mm	R	e%	P_d,GPa	$\dot{e}_t$, $10^3 sec^{-1}$	$\dot{e}$, $10^3 sec^{-1}$	T,°C
289.7	5.9	1.81	1.11	19	1.37	19.3	16.5	175
248.1	5.4	1.49	1.01	17	1.67	19.5	17.4	
213.1	5.	1.22	.99	16	1.81	18.8	17.2	
148.	4.4	.86	1.03	14	1.59	15.5	14.5	
96.5	3.6	.53	1.05	11	1.63	12.8	12.3	
56.2	2.7	.31	.99	9	1.86	10.3	10.0	

TABLE IX

PM A-703-1Y

Dynamic Test Data

V,m/s	w,mm	d,mm	R	eZ	P_d,GPa	$\dot{e}_t$, $10^3 sec^{-1}$	$\dot{e}$, $10^3 sec^{-1}$	T, °C
69.7	2.7	.22	1.36	9	2.85	12.7	12.5	25
64.3	2.6	.20	1.36	8	2.84	12.2	12.0	
102.7	3.3	.34	1.35	10	2.68	15.1	14.6	
100.3	3.3	.34	1.37	10	2.55	14.7	14.2	
154.6	4.1	.63	1.19	13	2.38	17.7	16.7	
158.3	4.2	.59	1.34	13	2.24	17.6	16.6	
208.5	4.o	.85	1.37	15	1.91	19.0	17.4	
246.7	5.4	1.09	1.39	17	1.65	19.4	17.3	
242.9	5.4	1.06	1.39	17	1.68	19.4	17.3	
279.9	6.0	1.30	1.65	19	1.14	17.9	15.1	
275.4	5.9	1.30	1.54	19	1.24	18.3	15.6	
44.6	2.4	.14	1.68	8	1.90	9.2	9.1	150
99.8	3.5	.38	1.37	11	1.78	13.0	12.5	
154.0	4.5	.66	1.42	14	1.55	15.7	14.6	
212.5	5.3	.98	1.46	17	1.35	17.2	15.4	
252.9	5.8	1.25	1.51	18	1.16	17.5	15.1	
299.3	6.3	1.61	1.73	20	.85	16.2	12.8	

TABLE X (con't)

V,m/s	w,mm	d,mm	R	eZ	P_d,GPa	$\dot{e}_t$, $10^3 sec^{-1}$	$\dot{e}$, $10^3 sec^{-1}$	NOTE
285.5	6.0	1.60	1.3	19	1.19	18.3	15.4	
81.2	2.9	.37	.94	9	2.88	13.7	13.4	

TABLE X

PM 7075

Dynamic Test Data

V,m/s	w,mm	d,mm	R	e%	P_d,GPa	$\dot{e}_t$, $10^3 sec^{-1}$	$\dot{e}$, $10^3 sec^{-1}$	NOTE
69.3	3.3	.41	1.1	10	1.22	10.2	9.8	-T0, 25°C
52.4	2.9	.30	1.2	9	1.20	8.9	8.6	
106.6	4.0	.65	1.1	13	1.26	12.5	11.9	
100.8	4.0	.63	1.1	12	1.19	12.0	11.5	
147.2	4.7	1.01	1.0	15	1.16	14.1	13.1	
147.2	4.7	1.03	1.0	15	1.16	14.1	13.1	
201.1	5.5	1.50	1.0	17	1.04	15.5	13.8	
207.0	5.6	1.55	1.1	18	.95	15.3	13.4	
237.4	6.0	1.86	1.1	19	.82	15.2	12.8	
238.	6.4	1.95	1.6	20	.44	11.7	8.8	
228.7	6.0	1.95	1.1	19	.76	14.6	12.3	
55.3	2.5	.21	1.2	8	2.47	11.0	10.8	-T6, 25°C
107.7	3.5	.41	1.2	11	2.29	14.8	14.2	
147.1	4.2	.59	1.3	13	1.94	16.3	15.4	
215.5	5.2	.95	1.4	16	1.53	17.9	16.2	
249.5	5.6	1.81	1.4	18	1.39	18.4	16.2	
288.	6.0	1.49	1.4	19	1.211	18.4	15.5	
5.8	2.7	.23	1.3	8	2.14	10.8	10.6	-T6,150°C
150.2	4.4	.70	1.3	14	1.64	15.7	14.7	
213.8	5.4	1.11	1.4	17	1.24	16.8	15.0	
252.8	5.8	1.37	1.4	18	1.16	17.4	15.1	

TABLE XI

PM 513-669-4B/6B

Dynamic Test Data, 25°C

V,m/s	w,mm	d,mm	R	e%	P_d,GPa	$\dot{e}_t$, $10^3 sec^{-1}$	$\dot{e}$, $10^3 sec^{-1}$	Heat Treat
72.2	2.9	.26	1.3	9	2.45	12.4	12.1	4B
92.3	3.2	.35	1.2	10	2.46	14.0	13.6	
154.1	4.2	.64	1.3	13	2.12	17.1	16.1	
152.6	4.2	.69	1.1	13	2.08	16.9	16.0	
210.1	5.	.97	1.3	16	1.76	18.5	16.9	
240.5	5.4	1.20	1.3	17	1.57	18.9	16.8	
61.6	2.8	.25	1.3	9	1.9	10.8	10.6	
48.2	2.4	.19	1.2	8	2.22	10.0	9.8	
282.8	6.	1.44	1.5	19	1.17	18.1	15.3	
285.7	6.	1.50	1.4	19	1.19	18.3	15.4	
282.	5.8	1.38	1.4	18	1.44	19.5	16.8	6B
262.1	5.8	1.37	1.4	18	1.25	18.1	15.6	
248.6	5.5	1.18	1.3	17	1.60	19.2	17.1	
249.7	5.5	1.15	1.4	17	1.53	19.	16.8	
205.4	4.9	.93	1.2	15	1.86	18.6	17.1	
202.4	4.9	.88	1.3	15	1.80	18.4	16.9	
151.8	4.2	.62	1.3	13	2.06	16.8	15.9	
140.4	4.2	.64	1.2	13	1.77	15.6	14.7	
98.6	3.4	.37	1.3	11	2.3	14.2	13.8	
100.1	3.3	.37	1.3	10	2.54	14.7	14.2	
63.	2.6	.22	1.3	8	2.73	120.	11.7	
76.	2.9	.27	1.2	9	2.75	13.2	12.9	

TABLE XII

PM 513-670-4B

Dynamic Test Data, 25°C

V,m/s	w,mm	d,mm	R	e%	P_d,GPa	$\dot{e}_t$, $10^3 sec^{-1}$	$\dot{e}$, $10^3 sec^{-1}$	NOTE
274.4	6.0	1.36	1.6	19	1.10	17.6	14.8	*
231.	5.6	1.13	1.5	18	1.19	17.0	15.0	*
215.2	4.9	.99	1.2	15	2.04	19.5	18.0	*
61.1	2.7	.23	1.3	9	2.19	11.2	10.9	
66.3	2.7	.23	1.3	9	2.58	12.1	11.8	
105.	33	.37	1.2	10	2.80	15.4	14.9	
99.9	3.4	.40	1.2	11	2.23	14.2	13.7	
164.	4.8	.73	1.5	15	1.31	15.3	14.1	+
165.6	4.4	.68	1.3	14	1.99	17.3	16.2	+
183.1	4.8	.81	1.3	15	1.71	17.3	16.0	*

* Fracture

+ Local Crater Edge Crack-Limit

TABLE XIII

2124-T3 W/SiO Whiskers (RT)

Dynamic Test Data, 25°C

V,m/s	w,mm	d,mm	R	e%	P_d,GPa	$\dot{e}_t$, $10^3 sec^{-1}$	$\dot{e}$, $10^3 sec^{-1}$	NOTE
72.6	3	.26	1.4	9	2.00	11.8	11.5	15%SiO
61.	2.8	.26	1.2	9	2.03	10.9	10.7	
104.1	3.6	.42	1.3	11	1.90	13.9	13.3	
103.9	3.6	.43	1.3	11	2.01	14.0	13.5	
150.6	4.2	.67	1.2	13	2.03	16.7	15.8	
154.6	4.4	.67	1.3	14	1.83	16.4	15.4	
205.	5.0	.97	1.3	16	1.68	18.1	16.5	
198.5	5.5	1.17	1.3	17	1.47	18.4	16.4	
242.1	5.5	1.18	1.3	17	1.51	18.7	16.6	
264.6	5.8	1.32	1.4	18	1.27	18.3	15.8	
234.9	5.9	1.31	1.5	19	.9	15.6	13.3	
68.6	2.8	.31	1.0	9	2.56	12.3	12.0	25%SiO
68.8	2.7	.30	1.0	9	2.78	12.6	12.3	
104.6	3.5	.47	1.1	11	2.16	14.4	13.8	
102.4	3.5	.48	1.1	11	2.07	14.1	13.5	
151.2	4.2	.71	1.1	13	2.16	17.0	16.1	
147.2	4.2	.73	1.1	13	2.04	16.6	15.7	
203.2	4.9	1.06	1.1	15	1.82	18.4	16.9	
196.7	4.9	1.07	1.1	15	1.70	17.9	16.4	
233.9	5.4	1.29	1.2	17	1.48	18.4	16.4	

TABLE XIII (con't)

V,m/s	w,mm	d,mm	R	e%	P_d,GPa	$\dot{e}_t$, $10^3 sec^{-1}$	$\dot{e}$, $10^3 sec^{-1}$	NOTE
227.2	5.4	1.33	1.1	17	1.47	18.1	16.2	
235.4	5.6	1.50	1.1	18	1.23	17.4	15.3	
245.3	5.5	1.51	1.1	17	1.48	18.7	16.5	

VITA

Captain Michael H. Bednarek was born on 17 April 1956 in Fox Lake, Wisconsin. He graduated form high school in Waupun, Wisconsin, in 1974 and attended the University of Minnesota from which he received the degree of Bachelor of Science in Aerospace Engineering and Mechanics in June 1978. Upon graduation, he received a commission in the USAF through the ROTC program. When called to active duty in August 1978, he entered the School of Engineering, Air Force Institute of Technology. (Upon leaving AFIT in March 1980, prior to course work completion, he was assigned to the Air Force Wright-Patterson Aeronautical Laboratories as an Aircraft Survivability and Vulnerability test engineer, and in May 1974 entered AFIT as a part-time student to complete degree requirements.

Permanent Address: Route 2, Box 15H
Niceville FL 32578

UNCLASSIFIED

SECURITY CLASSIFICATION OF THIS PAGE

REPORT DOCUMENTATION PAGE

1a. REPORT SECURITY CLASSIFICATION UNCLASSIFIED	1b. RESTRICTIVE MARKINGS
2a. SECURITY CLASSIFICATION AUTHORITY	3. DISTRIBUTION/AVAILABILITY OF REPORT Approved for public release; distribution unlimited.
2b. DECLASSIFICATION/DOWNGRADING SCHEDULE	
4. PERFORMING ORGANIZATION REPORT NUMBER(S) AFIT/GAE/AA/85M-1	5. MONITORING ORGANIZATION REPORT NUMBER(S)
6a. NAME OF PERFORMING ORGANIZATION School of Engineering 6b. OFFICE SYMBOL (If applicable) AFIT/ENY	7a. NAME OF MONITORING ORGANIZATION
6c. ADDRESS (City, State and ZIP Code) Air Force Institute of Technology Wright-Patterson AFB, OH 45433	7b. ADDRESS (City, State and ZIP Code)
8a. NAME OF FUNDING/SPONSORING ORGANIZATION AFWAL 8b. OFFICE SYMBOL (If applicable) FIESE	9. PROCUREMENT INSTRUMENT IDENTIFICATION NUMBER
8c. ADDRESS (City, State and ZIP Code) Wright-Patterson AFB, OH 45433	10. SOURCE OF FUNDING NOS. PROGRAM ELEMENT NO. / PROJECT NO / TASK NO / WORK UNIT NO.
11. TITLE (Include Security Classification) See Box 19	
12. PERSONAL AUTHOR(S) Michael H. Bednarek, B.S., Capt, USAF	
13a. TYPE OF REPORT MS Thesis 13b. TIME COVERED FROM _____ TO _____	14. DATE OF REPORT (Yr., Mo., Day) March 1985 15. PAGE COUNT 62
16. SUPPLEMENTARY NOTATION	

17 COSATI CODES			18. SUBJECT TERMS (Continue on reverse if necessary and identify by block number)
FIELD	GROUP	SUB GR	
20	11		Dynamic Plasticity, Hardness, Strain Rate Sensitivity,

19. ABSTRACT (Continue on reverse if necessary and identify by block number)

Title: STRAIN RATE SENSITIVITY ESTIMATION FROM HIGH VELOCITY IMPACT DATA

Thesis Chairman: George W. Watt, LtCol, USAF

Approved for public release: IAW AFR 190-17.

LYNN E. WOLAVER
Dean for Research and Professional Development
Air Force Institute of Technology (ATC)
Wright-Patterson AFB OH 45433

20. DISTRIBUTION/AVAILABILITY OF ABSTRACT UNCLASSIFIED/UNLIMITED ☒ SAME AS RPT ☐ DTIC USERS ☐	21. ABSTRACT SECURITY CLASSIFICATION UNCLASSIFIED
22a. NAME OF RESPONSIBLE INDIVIDUAL George W. Watt, LtCol, USAF	22b. TELEPHONE NUMBER (Include Area Code) 513-785-3517 22c. OFFICE SYMBOL AFIT/ENY

DD FORM 1473, 83 APR EDITION OF 1 JAN 73 IS OBSOLETE.

UNCLASSIFIED

SECURITY CLASSIFICATION OF THIS PAGE

This experimental study was designed to expand on the work accomplished by Sundararajan and Shewmon in estimating the strain rate sensitivity factors for various materials through the use of simple ballistic impact experiments. The study was divided into the following categories: development on an alternate method of estimating average strain rate, expand the existing data to include more relevant aerospace alloys, explore the effects of heat treatment or elevated temperatures on strain rate sensitivity, and to duplicate tests as a verification of assumptions.

The experimental procedure involved impacting test specimens with hardened steel spheres of known velocities, the resulting crater depth and diameter could then be correlated to an average strain rate. The energy of impact and crater volume can be equated to an average dynamic flow pressure.

The tests results compared favorably with those obtained by Sundararajan and Shewmon, however, their time of impact assumption resulted in errors exceeding 30% for high strain impacts while their crater relaxation profiles as a function of impact velocity was not justified for the materials tested.

General observations showed that the materials tested showed a variation in dynamic hardness with increased temperature and increased severity of heat treatment resulted in material less tolerant to strain rate variation. Strain rate sensitivity factors were low for the precipitated hardened alloys, intermediate for the solid solution alloys, and intermediate for the powered metal alloys. - Need Keywords included : see 1473

END

FILMED

7-85

DTIC